ELSEVIER

Contents lists available at ScienceDirect

# Science of the Total Environment

journal homepage: www.elsevier.com/locate/scitotenv





# Geomorphological controls on estuary hydrodynamics with implications for diatom blooms in deglaciated coastal areas

Taylor Bailey <sup>a,\*</sup>, Lauren Ross <sup>a</sup>, Nicholas Tiner <sup>a</sup>, Sean M.C. Smith <sup>a,b,c</sup>, Iván Ernesto Pérez Santos <sup>d</sup>, Antonio Ramos <sup>e</sup>, Alejandro García Mendoza <sup>e</sup>, David Miller <sup>f</sup>

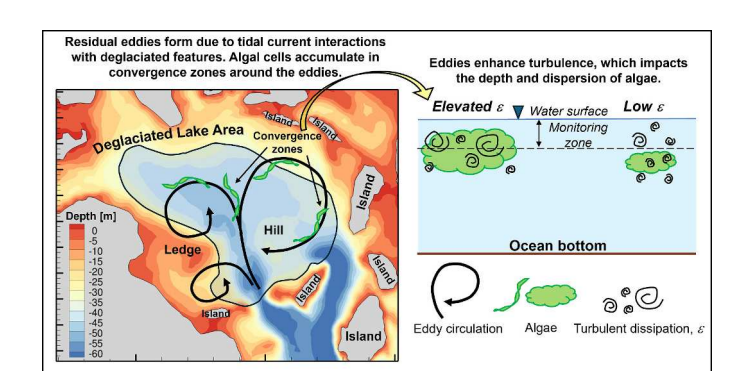
- a University of Maine, Department of Civil and Environmental Engineering, 5711 Boardman Hall, Orono, ME 04469, United States of America
- b University of Maine, School of Earth & Climate Sciences, 5790 Bryand Global Sciences Center, Orono, ME 04469, United States of America
- Esenator George J. Mitchell Center for Sustainability Solutions, 5710 Norman Smith Hall, Orono, ME 04469, United States of America
- <sup>d</sup> University of Los Lagos, i-mar Center, COPAS COASTAL and CIEP, Chile
- e University Institute ECOAQUA, Faculty of Marine Sciences, Campus de Tafira, 35017 Las Palmas de Gran Canaria, Spain
- f Maine Department of Marine Resources, 22 Coaling Station Ln, Lamoine, ME 04605, United States of America

#### HIGHLIGHTS

#### Local, small-scale (<5 km) circulation patterns influence algal sampling outcomes.

- Submesoscale (<10 km) eddies form due to deglaciated geomorphology.
- Near surface turbulence increased algal cell counts measured at the surface.
- Local algal cell accumulation occurs at tidal (<1d) and seasonal timescales.

#### GRAPHICAL ABSTRACT



#### ARTICLE INFO

Editor: Fernando Pacheco

Keywords:
Harmful algal blooms
Pseudo-nitzschia species
Eddies
Mixing
Nutrients
Deglaciation

#### ABSTRACT

Understanding local hydraulic conditions is imperative to coastal harmful algal bloom (HAB) monitoring. The research summarized herein describes how the locations and tidal phases selected for coastal hazard sampling can influence measurement results used to guide management decisions for HABs. Our study was conducted in Frenchman Bay, Maine, known for its complex deglaciated coastline, strong tidal influence, and shellfishing activities that are susceptible to problematic HABs such as those produced by some species (spp.) of the diatom genus *Pseudo-nitzschia*. In-situ measurements of current velocity, density, and turbulence collected over a semidiurnal tidal cycle and a companion numerical model simulation of the study area provide concurrent evidence of two adjacent counter-rotating sub-mesoscale eddies (2–4 km diameter) that persist in the depth-averaged residual circulation. The eddies are generated in the wake of several islands in an area with abrupt bathymetric gradients, both legacy conditions partly derived from deglaciation ~15 kya. Increased concentrations of *Pseudo-nitzschia* spp. measured during the semidiurnal survey follow a trend of elevated turbulent dissipation rates near the water surface, indicating that surface sampling alone might not adequately indicate

<sup>\*</sup> Corresponding author at: University of Maine, 5711 Boardman Hall, Orono, ME 04469, United States of America *E-mail address*: taylor.l.bailey@maine.edu (T. Bailey).

species abundance. Additional measurements of *Pseudo-nitzschia* spp. from two years of weekly sampling in the region show that algal cell abundance is highest where residual eddies form. These findings provide incentive to examine current practices of HAB monitoring and management by linking coastal geomorphology to hydraulic conditions influencing HAB sampling outcomes, coastal morphometric features to material accumulation hotspots, and millennial time scales to modern hydraulic conditions.

#### 1. Introduction

Harmful algal blooms (HABs) are a relevant concern for coastal shellfishing activities, such as aquaculture and harvesting, because many species of HABs produce toxins that accumulate in shellfish and can cause illness when consumed by humans. For instance, some species of the marine diatom genus Pseudo-nitzschia can produce domoic acid, a biotoxin responsible for Amnesic Shellfish Poisoning, a neurological syndrome that can potentially be fatal (Bates et al., 2018). Coastal water circulation and mixing have been found to influence HAB growth and transport in estuaries (Glibert et al., 2005; Gentien et al., 2005; Pitcher et al., 2010; Qin and Shen, 2019) and therefore have direct implications for monitoring and management strategies surrounding HABs. Previous studies have linked rotational circulation patterns described as "eddies" to the retention and transport of HABs along the west coast of North America (Anderson et al., 2006). One such eddy, the Juan de Fuca Eddy off the Washington state coast, is an example of a seasonally varied, mesoscale (horizontal scales on the order of ~10-100 km) eddy with a diameter of ~30-60 km that has been found to influence HAB dynamics (Trainer et al., 2002, 2009; MacFadyen et al., 2005, 2008). Greater focus on smaller-scale eddies (sub-mesoscale eddies, under 10 km diameter), particularly near coastlines, is necessary because of the concomitant increases in seafood farming (FAO, 2022) and prevalence of HABs around the world (Anderson, 2009). At present, regulatory monitoring for HABs, which often informs the spatial extent of regional closures to shellfishing activities, is typically localized over small spatial scales. Knowledge of the connections between localized geomorphic conditions, modern tidal hydraulic conditions, and physical HAB dynamics is therefore necessary to advance coastal monitoring and management strategies in complicated estuary sub-embayment areas with shellfish harvesting activities.

Geomorphic features such as islands, headlands, and bathymetric gradients can influence tidal hydraulic conditions by steering flows and producing vorticity (i.e. rotation of the flow) in localized areas (Zimmerman, 1978; Pingree, 1978; Pingree and Maddock, 1980; Zimmerman, 1981; Geyer and Signell, 1990; Signell and Geyer, 1991). Locations of accentuated vorticity that appear as eddies can be transient, manifesting only on specific phases of the tide (e.g. Trinast, 1975; Geyer and Signell, 1990; Signell and Geyer, 1991; Brooks et al., 1999) or under specific weather conditions (Li and Weeks, 2009). The vorticity created by the tidal flows can manifest in the mean (residual) flow to produce tidal residual eddies (Pingree, 1978; Zimmerman, 1978; Robinson, 1981; Zimmerman, 1981). These eddies can impact exchange between an estuary and the ocean (e.g. Yang and Wang, 2013), and therefore have consequences for material transport and sampling outcomes, of particular concern in relation to monitoring for shellfish management purposes during HAB events. Moreover, eddies can exacerbate HABs in coastal zones by limiting the advection of phytoplankton (MacFadyen et al., 2008; Qin and Shen, 2019), enhancing growth by bringing essential nutrients to the surface (Coria-Monter et al., 2017) and possibly even increasing toxicity by entraining blooms in nutrientlimited zones (Anderson et al., 2006). These dynamics raise concern for the susceptibility of areas with complex coastlines to HAB events. Further, HAB monitoring programs often conduct sampling on a weekly basis (Anderson et al., 2001), which is too infrequent to resolve the influence of some physical processes on bloom formation, like tides and the localized circulation patterns that form on specific tidal phases.

Eddies generated by flow interactions with geomorphic features such

as headlands can produce near-surface mixing decoupled from sheardriven mixing near the bottom of an estuary (Spicer and Huguenard, 2020). As vertical mixing in the water column can influence the distribution of material suspended there, an enhancement of near-surface mixing would allow the upper water column to become increasingly homogenized, and for material to be advected to and from the surface. Further, tidal flow interactions with bathymetric features can induce vorticity and mixing that can transport materials from deeper in the water column to the surface. This effect was observed in the Gulf of California, where the upward flux of nutrients increases phytoplankton concentrations near the surface (Salas-de-León et al., 2011). Despite the known influence of vertical mixing on advection of suspended materials, consistent associations between coastal geomorphology, circulation patterns, timing and locations of enhanced mixing, and monitoring for HABs remain to be specifically identified, especially over small spatial (<10 km) and temporal (<1 d) scales.

Coastal Maine (USA) is characterized by estuary conditions shaped by the mechanical work of deglaciation ~15 kya (Borns et al., 2004). Consideration of the interactions between coastal geomorphologic features and tidal currents is particularly relevant to the area given the complicated conditions left behind by glacial erosion and deposition processes. Maine has approximately ~5,600 km of rugged coastline and a growing aquaculture industry that is facing increasing vulnerability to HAB events (Bates et al., 2018). This vulnerability creates a demand for a better understanding of circulation and mixing dynamics in the embayments and estuaries along the coast of Maine to support decision making related to fisheries management. Accordingly, the goal of this study is to connect coastal geomorphological features to modern local hydraulic conditions and outcomes from estuary water sampling approaches similar to those used to monitor HAB events affecting shellfishing activities. Three primary objectives were targeted to direct this study: 1) Quantification of estuary circulation and mixing patterns over the duration of a tidal cycle in a location governed by hydraulic forcings from coastal geomorphological features; 2) Identification of the linkages between estuary circulation and mixing patterns to specific coastal bedrock landforms, estuary bathymetry, and tidal conditions; and 3) Examination of the associations between local hydraulic conditions and concentrations of suspended and dissolved constituents collected in water samples, specifically phytoplankton cells and nutrients.

The remainder of this manuscript will include a description of our study site, Frenchman Bay, which is located near Acadia National Park, in Section 2. In Section 3 we describe the methodology of our study, and in Section 4 we present and discuss our results, highlight the implications of our findings for monitoring and management of HABs, and discuss the limitations of our study. Conclusions based on our results are drawn in Section 5.

#### 2. Study site

In 2016, toxic *Pseudo-nitzschia australis* (*P. australis*) cells were detected in estuaries and coastal embayments in the Gulf of Maine for the first time, forcing the Maine Department of Marine Resources (MEDMR) to make extensive closures of the regions estuaries to shellfish harvesting and aquaculture farming (Bates et al., 2018; Clark et al., 2019). *P. australis* is one of the 26 species of *Pseudo-nitzschia* known to release domoic acid, the biotoxin responsible for the potentially lifethreatening illness Amnesic Shellfish Poisoning (Bates et al., 2018). Our study focuses on Frenchman Bay, Maine, a region within the Gulf of

Maine (Fig. 1a) that was impacted by the 2016 HAB event. Located next to Acadia National Park on Mount Desert Island (Fig. 1b), Frenchman Bay has significant economic and social importance. Local fishermen depend on the bay for its economically prolific shellfish harvesting, lobstering, and aquaculture industries. At present, there are over forty active permitted or leased aquaculture areas in Frenchman Bay and its surrounding estuaries (Maine, 2022a – accessed 12/04/2023). These lease sites are susceptible to emergency harvesting closures due to the detection of biotoxins produced by HABs during weekly regulatory biotoxin monitoring (Maine, 2022b).

The mechanical work of glacial advance and retreat of the Laurentide ice sheet resulting from the last ice age shaped the contemporary coastal terrain and waterways around Mount Desert Island (Borns, 1973 and references therein; Borns et al., 2004; Braun and Braun, 2016). After glacial retreat and land rebounding (nearly 14,000 years ago), Frenchman Bay was elevated above sea level and became a glacial lake, lending to the sharp bathymetric gradients and numerous islands that are features of the bay today (Braun and Braun, 2016; Borns et al., 2004). Several islands (i.e., Porcupine, Ironbound, Jordan, and Stave Islands) form a chain near the entrance of the bay in a location coincident with a remnant glacial lake shoreline. Carved between these islands

are deep channels, reaching depths of over 90 m (Fig. 1b). The bay itself is roughly 11 km long (north to south) and 23 km wide (east to west). The tides are semidiurnal ( $\sim$ 12 h) dominant with an amplitude of approximately 2.16 m based on a tide gauge station at Bar Harbor (Fig. 1b; Alahmed et al., 2022). The tidal range for this area varies fortnightly, with a maximum range of 4.5 m during the spring tide and 2 m during the neap tide (Davies, 1964).

Frenchman Bay receives freshwater from numerous streams but has relatively low cumulative inflow from these sources. The most notable input comes from the Union River, located on the western side of Mount Desert Island (MDI), which contributes an annual average flow of  $\sim\!28$   $m^3s^{-1}$  to the region (Alahmed et al., 2022). The water on the western side of Frenchman Bay is exchanged with that of the eastern side of Frenchman Bay only through a narrow channel ( $\sim\!40$  m, measured using Google Earth) located to the north of MDI (Fig. 1b). Other sources of freshwater input on the eastern side of MDI (to the east of the narrow channel in Fig. 1b) total an average annual discharge of  $<\!10$  m $^3s^{-1}$ , estimated using the United States Geological Survey (USGS) StreamStats flow estimates for nine of the main tributaries in the region (streams 1–9 in Fig. 1b; U.S. Geological Survey, 2019; https://streamstats.usgs.gov/ss/ - accessed 7/10/23). Flows estimated by StreamStats are

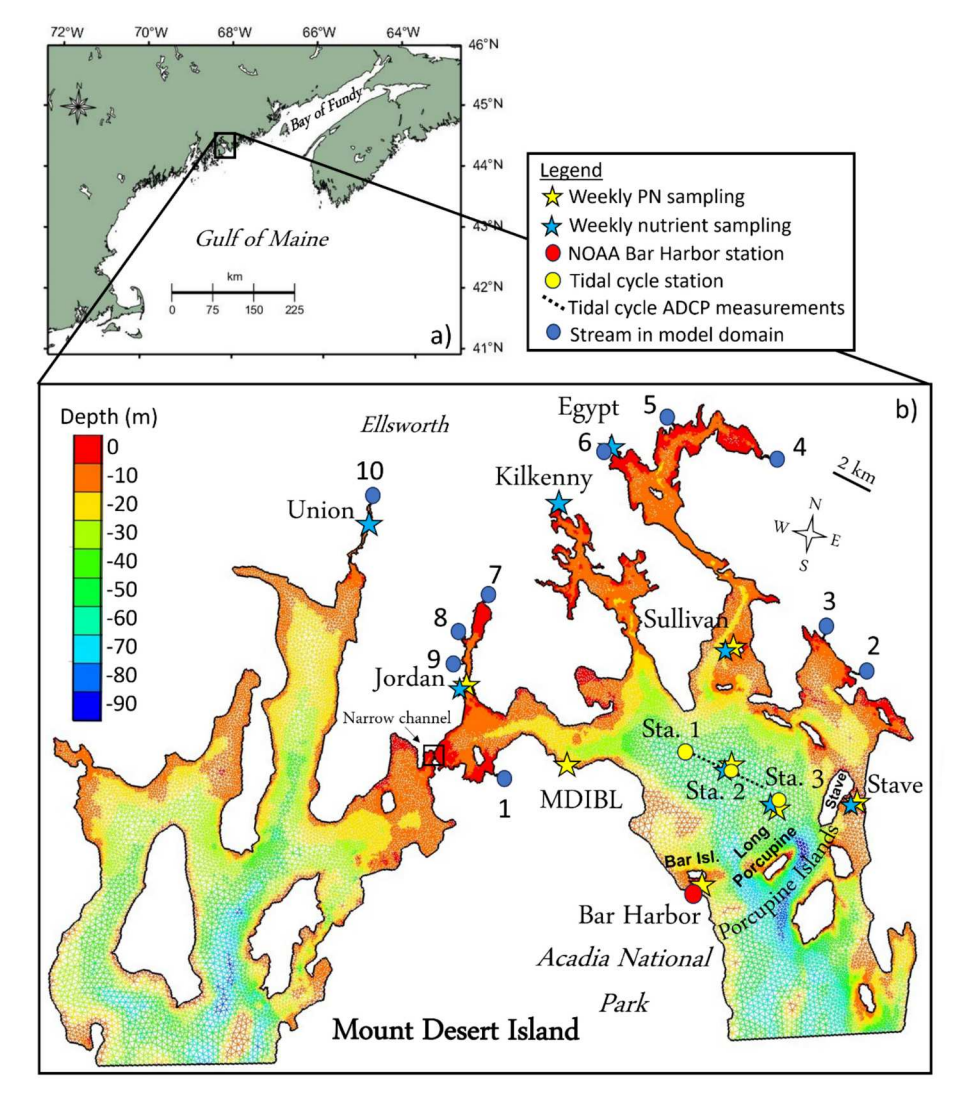


Fig. 1. a) Study region relative to the Gulf of Maine. b) Numerical model domain showing the bathymetry of the region, with stream boundaries (blue dots) numbered 1–10. Also shown are the sampling locations for the tidal cycle survey measurements on June 15th, 2022, Stations 1, 2, and 3 and the ADCP transect (black, dashed line), and the locations of weekly sampling (blue and yellow stars). Note that the weekly sampling stations include three 'stream stations': Union, Kilkenny, Egypt; three 'nearshore stations': Jordan, Sullivan, Stave; and two 'bay stations': Station 2 and Station 3. In the legend, PN stands for *Pseudo-nitzschia* spp. Panel a) map source: M\_Map software (Pawlowicz, 2020).

generated following the method of Dudley (2015). The nine tributaries considered in this estimate and Union River are included as freshwater boundaries in the numerical model domain (blue dots in Fig. 1b), the details of which are presented in Section 3.2 (see also Table A1 in the Appendix for monthly average discharges for these streams).

#### 3. Methods

#### 3.1. Tidal cycle measurements

Data were collected along a ~4 km transect on June 15th, 2022 (Fig. 1b) under calm wind conditions, with max gusts under 6 m/s (National Oceanic and Atmospheric Administration [NOAA], n.d.; https://tidesandcurrents.noaa.gov/met.html?id=8413320, not shown). No precipitation was received in the area on this day, nor was any received in the few days preceding it (National Centers for Environmental Information [NCEI], n.d.; https://www.ncei.noaa.gov/cdo-web/ datasets/LCD/stations/WBAN:14616/detail, not shown). It is therefore assumed that wind and freshwater forcing were minimal during this field campaign, and that tidal forces dominated. North-South (N-S) and East-West (E-W) current velocity profiles were collected throughout the water column with a vessel-towed 300 kHz RDI Workhorse Acoustic Doppler Current Profiler (ADCP). The ADCP measured in 1 m vertical bins at a rate of two pings per ensemble, and the transect was sampled 16 times (measuring from one end of the transect to the other each time) to capture a full semidiurnal tidal cycle. Incorporation of a Garmin GPS into the ADCP software allowed for the exact location of the velocity measurements to be recorded.

While one vessel towed the ADCP, another vessel traveled back and forth along the transect stopping to collect data with a Rockland Scientific Conductivity, Temperature, and Depth (MicroCTD) profiler at three stations (Fig. 1b). Station 1 is on the western end of the ADCP transect, Station 2 is in the center of the transect and Station 3 is at the eastern end of the transect. Stations 2 and 3 were strategically chosen as they are two of the five locations where *Pseudo-nitzschia* spp. data were collected weekly during the summer and fall months of 2021 and 2022 (Fig. 1b, see Section 3.4). During the tidal survey, the MicroCTD was cast off the boat at least five times each time the vessel stopped at a station to measure velocity shear with two accelerometer probes affixed to the instrument. Some discrepancies in the position of the ADCP data and the MicroCTD data exist because the research vessel towing the ADCP maintained a speed <2.5 knots to continuously measure currents. Velocity shear measurements from the MicroCTD were sampled at a rate of 512 Hz and were converted to turbulent kinetic energy dissipation,  $\varepsilon$ , that is a proxy for shear-driven mixing (see Section A1 in the Appendix for details; also see the methodology of Ross et al., 2019 and references therein). The MicroCTD also sampled chlorophyll-a at a rate of 512 Hz, and salinity and temperature at a rate of 64 Hz, with the objective to obtain five depth profiles to be averaged together to provide one representative profile for each metric. The chlorophyll-a fluorescence measured by the fluorometer affixed to the MicroCTD was not validated using discrete in-situ chlorophyll samples. For details of the processing of the hydrographic data and velocities see Section A2 in the Appendix. For the conversion of salinity and temperature to density and the calculation of the buoyancy frequency,  $N^2$ , and the potential energy anomaly,  $\phi$ , used to describe the stratification of the water column, see Section A3 in the Appendix.

Surface water samples were collected and filtered on the same vessel as the MicroCTD per the Maine Department of Marine Resources (MEDMR) sampling protocol (personal communication with MEDMR, June 16, 2021) to quantify *Pseudo-nitzschia* spp. cell counts at Station 2 and Station 3 (Fig. 1b). Twice as many measurements were collected at Station 2 compared to Station 3 over the tidal cycle due to the sampling pattern along the transect. For each sample, approximately 10 L of seawater were filtered through a 20 µm sieve to capture phytoplankton. The sieve was then inverted over a funnel attached to a 50 mL tube, and

backwashed with seawater spray collected at the site until the sample was diluted to a volume of approximately 15 mL. All sampling equipment was thoroughly rinsed three times in seawater local to the sampling station before the filtering process began to mitigate cross-contamination. The *Pseudo-nitzschia* spp. samples were stored in a cooler with ice packs maintained between 0 and 10 °C for the remainder of the sampling. Further information on the treatment and analysis of the *Pseudo-nitzschia* spp. cells collected during the tidal cycle survey and the weekly sampling (described in Section 3.4) is included in the Appendix (see Section A4).

#### 3.2. Hydrodynamic simulations

To investigate the regional circulation patterns at larger spatial scales, a TELEMAC-MASCARET three-dimensional (Telemac3D) model (Fig. 1b) was used to perform a numerical simulation of the tidal cycle surveyed on June 15th, 2022. This model configuration has been validated and used in previous studies in the same area (Ross et al., 2021; Alahmed et al., 2022), however for the present study, the depth-averaged (two-dimensional) model output was used for validation and analysis. The water levels measured by the tide gauge at the Bar Harbor station (Fig. 1b) were revalidated for approximately two weeks preceding and including the survey date, producing a skill score of 0.99 (Willmott, 1981). The flow velocity at Stations 1, 2, and 3 were also validated against the ADCP measurements on June 15th, 2022, producing skill scores >0.85 (not shown).

Astronomical tidal forcing was included at the ocean boundaries in the model via the TPXO database (Egbert and Erofeeva, 2002). Monthly average stream inflow rates from the ten tributaries included in the model domain (Fig. 1b) were estimated by USGS StreamStats based on the method of Dudley (2015) (U.S. Geological Survey, 2019; https://st reamstats.usgs.gov/ss/ - accessed 6/13/23). The flow rates provided the upstream boundary conditions for the simulations (see Table A1 in the Appendix and Alahmed et al., 2022). Hourly wind speed and direction measured at the Bar Harbor station (NOAA, n.d.; https://tide sandcurrents.noaa.gov/met.html?id=8413320; Fig. 1b) provided wind forcing for the simulation. A six-month simulation "spin-up" was implemented to stabilize the salinity field, assuming a constant salinity of 32 PSU at the ocean boundary. The model simulation was run with a time step of 10 s with model output saved every 30 min for analysis. More details regarding the model configuration are summarized in Alahmed et al. (2022).

### 3.3. Satellite imagery

Sentinel-2B Multi-Spectral Instrument (MSI) data were examined in the coast of Maine and in Frenchman Bay on the date of the tidal cycle survey (June 15th, 2022) to identify the presence of algae. Raw data and images of Sentinel-2B were downloaded from Sentinel Data Hub with a revisiting cycle of 5 days. The Level 2A products were downloaded in only one of the 9 granules of Sentinel 2B (100 km  $\times$  100 km) obtained for the coast of Maine, that showed the presence of microalgae filaments (the T19TEK). The image was processed with the standard bottom-ofatmosphere reflectance profiles for each radiometric band, and were then georeferenced in cartographic geometry coordinates with the standard SEN2COR library of atmospheric correction algorithms provided by the scihub Copernicus for both Sentinel 2A,B (https://step.esa. int/main/snap-supported-plugins/sen2cor/). The RGB corrected scene (bands 12, 8, and 3) was finally selected to target the microalgae held along the coastal waters of Maine off Mount Desert Island and in the study area of Frenchman Bay.

#### 3.4. Weekly sampling

In addition to the tidal cycle sampling on June 15th, 2022, *Pseudo-nitzschia* spp. abundance and nutrient samples were collected weekly

during the summer and early fall (July–October; 14 weeks total) of both 2021 and 2022, corresponding to the months in which the 2016 *Pseudonitzschia* spp. bloom occurred in the Gulf of Maine (Clark et al., 2019). Sampling occurred on the day of the week with the "best weather conditions" when wind velocities were low ( $\sim$ <6 m/s), and preferably when there was little or no precipitation. However, the river and stream flow conditions before and during the chosen sampling day varied. In addition, the tidal phase during sampling was random, depending on the chosen sampling day, making the data representative of all tidal and freshwater discharge conditions.

Pseudo-nitzschia spp. samples were collected weekly following the same methodology as described for the tidal cycle survey (Section 3.1) at five locations in Frenchman Bay, including two 'bay stations' called Station 2 and 3 and three 'nearshore stations' named Stave, Sullivan, and Jordan after the estuaries within which they are located (see Fig. 1b). In addition to the data collected at these five sampling stations, Pseudo-nitzschia spp. counts measured during the MEDMR regular seasonal monitoring program are available in an online repository (https://mainedmr.shinyapps.io/bph\_phyto/) for these years. Their data were collected approximately weekly at two stations within our study region, Bar Harbor and Mount Desert Island Biological Laboratory (MDIBL; see Fig. 1b), and were included in our analysis. The sampling frequency at these stations varied compared to our weekly sampling, resulting in different sample sizes (n) in the means (for 2021, n = 15 for MDIBL and n = 13 for Bar Harbor; for 2022, n = 9 for MDIBL and n = 17for Bar Harbor), and only data collected during the weeks of our sampling season were included in our analysis. In the remainder of the text, the MDIBL and Bar Harbor stations will be referred to as 'nearshore stations' along with the Stave, Sullivan, and Jordan stations, however only Pseudo-nitzschia spp. data (not nutrient data) are available at these locations, as they were not a part of our sampling campaign.

Water samples for nutrient analysis were also collected during the weekly sampling in 2021 and 2022. These samples were shipped to the Virginia Institute of Marine Science (VIMS) Analytical Services Center, a VELAP (Virginia Environmental Laboratory Accreditation Program) certified laboratory for analysis (VIMS quality manual and test methods can be found here: https://www.vims.edu/research/facilities/asc/). Samples were collected in clean bottles and triple-rinsed in the local seawater at each site prior to collection. During transportation the samples were kept in a cooler with ice packs, and upon return to the laboratory samples were moved to a freezer until shipment to VIMS. Samples were analyzed at VIMS to measure total dissolved nitrogen (TN) and total dissolved phosphorus (TP) concentrations during both 2021 and 2022. Quantification of ammonia (NH<sub>3</sub>), nitrate+nitrite (NO<sub>x</sub>), and silica (SiO2) was also conducted on samples collected in 2022. Concentrations of TN, NH3, and NOx were reported by VIMS as mg/L-Nitrogen (N), concentrations of SiO2 as mg/L-Silicon (Si), and concentrations of TP as mg/L-Phosphorus (P). In both years, nutrient sampling was conducted at the 'bay stations', Stations 2 and 3, at the 'nearshore stations' Stave, Sullivan and Jordan, and additionally at three other stations located near the mouths of freshwater streams that enter the bay. These 'stream stations' are named Union, Kilkenny, and Egypt (Fig. 1b). The Sullivan, Jordan and Stave 'nearshore stations' were located within aquaculture lease areas owned by stakeholder partners where monitoring for toxic Pseudo-nitzschia spp. and water quality conditions is of vital importance for shellfish management. Collectively, the weekly sampled data augment capacity to describe ambient conditions of Pseudo-nitzschia spp. and nutrients in the study area. Further summary of the sampling locations and the types of data collected at each station is provided in the Appendix (see Table A2).

# 3.5. Statistical analyses

# 3.5.1. Tidal cycle measurements

Trends between surface measured *Pseudo-nitzschia* spp. data and turbulent dissipation ( $\varepsilon$ ) measured during the tidal cycle survey were

assessed by a Pearson correlation. This calculation was performed using the MathWorks software, MATLAB. To utilize the Pearson correlation, the data must be normally distributed. The distribution of the *Pseudonitzschia* spp. data was assumed to be normal, after failure to reject the null hypothesis in an Anderson-Darlings test, performed using MATLAB. The  $\varepsilon$  near the surface was also assumed to be normally distributed after transforming onto a base 10 log scale.

#### 3.5.2. Weekly sampling

To assess whether nutrients measured from the weekly sampling significantly influence the abundance of Pseudo-nitzschia spp., we computed the sample cross-correlation function of Pseudo-nitzschia spp. versus nutrient concentrations. This analysis was performed using the MATLAB sample cross-correlation function by MathWorks, which is based on the method of Box et al. (1994) and has been used for this purpose in other studies (Morse et al., 2014). Due to the variability in the sampling interval of the "weekly" sampled data, which was not always exactly seven days due to restrictions caused by weather conditions, the lag is reported in days between the sampling dates. An increase in diatom abundance is known to lag an increase in relevant nutrient concentrations (Morse et al., 2014; Gilpin et al., 2004), therefore only a positive lag (Pseudo-nitzschia spp. lagging nutrient concentrations) was considered. Further, only a lag of up to 20 days (period of three sampling weeks) was deemed relevant because diatom growth rates are on the order of days (Morse et al., 2014), and nutrient depletion by diatoms has been shown to occur within 4-12 days (Gilpin et al., 2004). The 95 % and 85 % confidence intervals (CI) for the correlations were calculated for using the formula,  $\pm z/\sqrt{n-k}$ , where z is the number of standard errors from the mean, n is the number of samples considered at the lag, and k is the number of the lag (e.g. k = 1 represents a lag of approximately seven days). The MATLAB sample cross-correlation function computes the confidence bounds as  $\pm z/\sqrt{n}$ , however this does not account for a reduction in the sample size with increasing lag, and therefore CI were computed after the fact.

#### 4. Results and discussion

#### 4.1. Tidal cycle measurements

## 4.1.1. Stratification and turbulent dissipation

The goal of this study is to link coastal geomorphological features to local circulation patterns and HAB monitoring outcomes. We first consider these linkages over the tidal cycle captured just after the start of flood tide on June 15th, 2022. Temperature varied up to 5 °C between the surface layer and the bottom (Fig. 2b(1–3)). The top-to-bottom salinity difference was small, <1 PSU (Figs. 2c(1–3)), indicating that the water column was relatively well-mixed with slight variations in vertical stratification conditions throughout the tidal cycle at each station as indicated by buoyancy frequency,  $N^2$  (Fig. 2d(1–3)) and potential energy anomaly,  $\phi$  (Fig. 2e(1–3)). Based on values of  $\phi$ , water column stratification also varied spatially along the transect, with stratification weakening from station 1 to 3. Gaps in salinity,  $N^2$ , and  $\phi$  (Fig. 2c(2), 2d (2), and 2e(2) respectively) are the result of the removal of salinity cast measurements from the dataset because of instrument interference with the bottom, or density instabilities in the case of  $N^2$  (Fig. 2d(3)).

At Station 1, turbulent dissipation,  $\varepsilon$ , was high ( $\sim 10^{-7}$  W/kg) near the surface (upper 15 m depth) during flood tide (Fig. 2f(1)).  $N^2$  was elevated indicating a pycnocline (Fig. 2d(1)) at  $\sim 20$  m that limited the strength of  $\varepsilon$  below at this time. The pycnocline was closer to the surface ( $\sim 10$  m) during slack after flood ( $\sim 16-17$  h), further limiting the depth of high  $\varepsilon$  and the vertical extent of the relatively warm surface layer (Fig. 2b(1)). Results at Station 2 show that  $\varepsilon$  was elevated ( $> 10^{-7}$  W/kg) throughout the water column, but only during late flood tide ( $\sim 15$  h; Fig. 2f(2)). The  $\phi$  was relatively low during this time as expected since greater dissipation contributes to the breakdown of stratification (Fig. 2e).

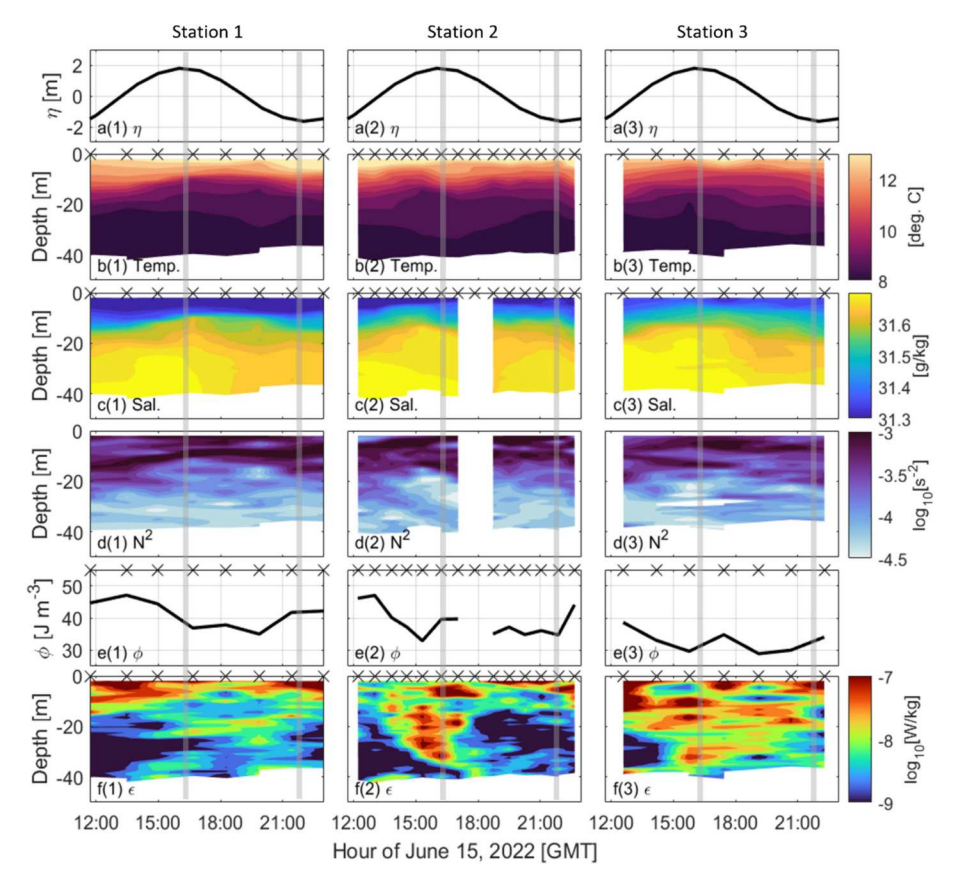


Fig. 2. Columns 1, 2 and 3 show the following conditions at Stations 1, 2, and 3 respectively: a(1-3) Variation in the water level observed at the NOAA Bar Harbor station (see Fig. 1b), shown three times for ease of reference to the hydrographic variables at each station. b(1-3) temperature, c(1-3) salinity, d(1-3) squared buoyancy frequency, e(1-3) potential energy anomaly, and f) turbulent dissipation. The x's on top of panels denote times of the MicroCTD casts. The light gray lines approximately denote the slack tide after flood and slack tide after ebb. Large gaps in data in panels c(2), d(2), and e(2) are a result of the removal of bad casts from the salinity data. Gaps in panel d(3) are the result of density instabilities, possibly caused by measurement error.

(2)). At Station 3,  $\varepsilon$  was symmetric throughout the tidal cycle and was overall higher throughout the water column and tidal cycle when compared to the other stations (Fig. 2f(3)). Highest values of  $\varepsilon$  at Station 3 corresponded to low values of  $\phi$ , which reached a minimum of  $\sim$ 30 J m<sup>-3</sup> during slack tide after flood ( $\sim$ 16 h; Fig. 2e(3)). The pycnocline was less defined at Station 3 than at Station 1 or 2, due to elevated  $\varepsilon$  throughout the water column. Overall, a pronounced intratidal variability in  $\varepsilon$  was only observed at Station 2.

Instances of elevated  $\varepsilon$  were predominantly located in the upper to mid water column at all stations, uncoupled from bottom-generated shear. Similar conditions have been observed from eddy formation processes documented in other studies (Spicer and Huguenard, 2020). Some have shown that vorticity and vertical mixing occur simultaneously due to high velocity shear generated by tidal currents interacting with bathymetric features (Salas-de-León et al., 2011). We present the observed tidal currents next to investigate if this could be the case in Frenchman Bay.

#### 4.1.2. Current velocities

The circulation structure suggests the presence of transient eddies which we hypothesize form due to the geomorphology of the region. The timing of eddy formation during late flood tide ( $\sim$ 15–16 h) and slack tide after flood ( $\sim$ 16–17 h) in the current velocities corresponds well with the timing of elevated  $\varepsilon$  at the middle of the transect (Station 2, Fig. 2f(2)). The bay experienced lateral shear of the along-channel flow throughout the tidal cycle, but most prominently during flood tide due to the divergence of tidal currents in the bay and flow separation in the wake of the island chain. During flood tide, currents were predominately directed to the northwest throughout the water column (Fig. 3B(a-b)).

The depth-averaged velocity vectors (Fig. 3C) depict strong northwest directed flows on the eastern side of the bay during flood tide (transects 1–5), and weaker northwest directed flows on the western side of the bay.

The depth-averaged velocity vectors (Fig. 3C) along transects measured during slack tide after flood (transects 6–9) revealed a relatively large-scale rotation of the flow on the eastern side of the bay. Flows that were directed to the northwest at the end of flood tide (transects 5–6) turned clockwise during the slack tide to be directed to the southeast by the beginning of ebb ( $\sim$ 19 h). The currents were weaker on the western end of the transect (Fig. 3B(c-d)), but the change in direction of the depth-averaged velocity vectors (Fig. 3C) suggests a rotation in the opposite direction (counterclockwise) from northwest directed at the end of flood to southeast directed by the beginning of ebb. The currents are directed to the southeast on ebb tide with strongest current velocities on the western side of the transect (Fig. 3C,  $\sim$ 20 h) due to the orientation of the bay.

The measured transect current velocities indicate the presence of eddies, with a large eddy forming on the eastern side of the bay after flood tide. The presence and timing of this eddy help to explain the variability in  $\varepsilon$  along the transect. Station 1, located on the western end of the transect, is outside of this large eddy and has relatively low  $\varepsilon$  throughout the water column and tidal cycle compared to the other stations (Fig. 2f(1)). Station 2 is located between the two eddies at the center of the bay where the deep channel steers the tidal flows. Station 3 is located on the eastern end of the transect at the periphery of the large eddy. The presence of this large eddy might cause  $\varepsilon$  to be consistently elevated throughout the tidal cycle. Because of their proximity to the large eddy structure, we will focus on Stations 2 and 3. The following

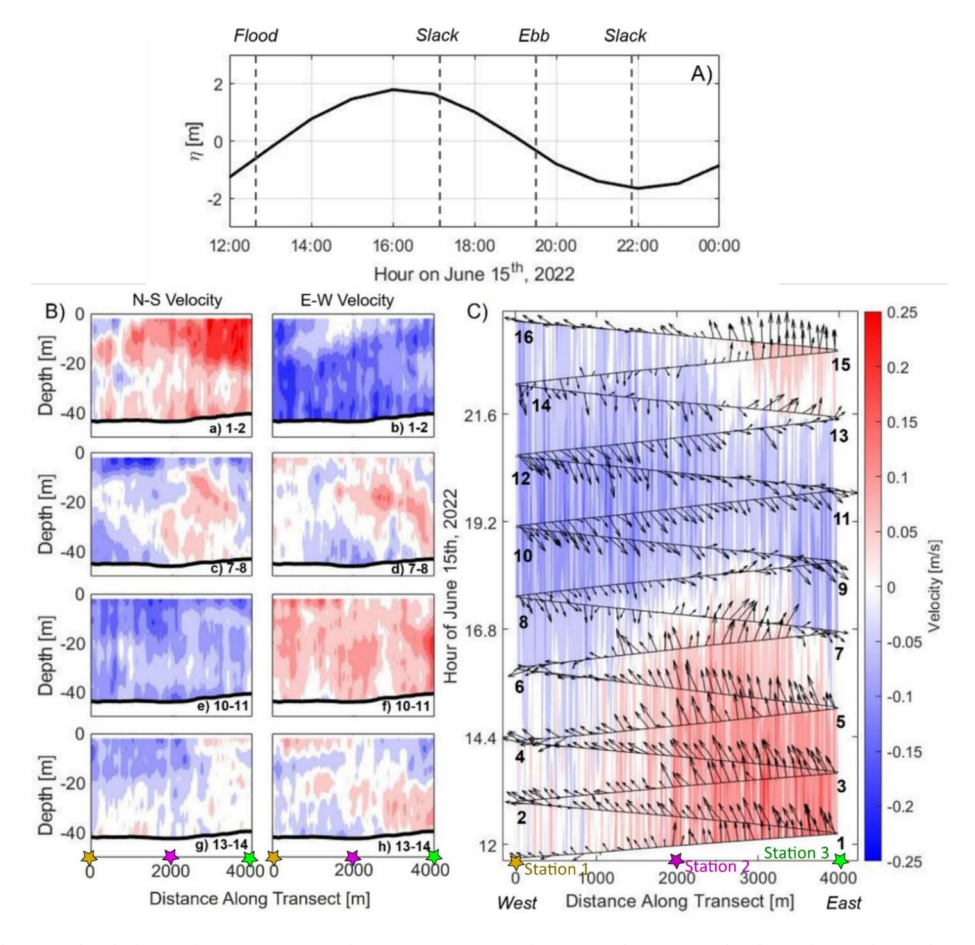


Fig. 3. A) Variation in the water level observed at NOAA Bar Harbor station (see Fig. 1b). B) Panels a, c, e, and g (left column) depict the North-South velocities with depth for select transects in C. Positive (red) velocities are directed to the north (into the bay) and negative (blue) velocities to the south (out of the bay). Panels b, d, f, and h (right column) depict East-West velocities with depth for those transects. Positive velocities are to the east and negative velocities are to the west. The magnitude of the flows corresponds to the color bar in C. C) Depth-averaged velocity vectors on top of the depth-averaged velocity magnitude for all measured transects. The stars at the bottom of the subplot indicate the Station 1 (brown star), Station 2 (purple star) and Station 3 (green star) data collection sites that correspond to Fig. 2.

subsection will link the intratidal patterns in  $\varepsilon$  to *Pseudo-nitzschia* spp. abundance at these stations.

## 4.1.3. Turbulent dissipation & Pseudo-nitzschia spp. abundance

Pseudo-nitzschia spp. abundance was determined from surface water samples collected at Stations 2 and 3 throughout the tidal cycle (Fig. 4b) (1–2)). Chlorophyll-a and  $\varepsilon$  measurements were collected with the MicroCTD at the same two locations to complement the in-situ species cell counts (Fig. 4c(1-2)). At Station 2, chlorophyll-a concentration was primarily above 20 m depth, except at slack after flood tide (15-17 h), at which time the concentration extended to 25 m depth (Fig. 4c(1)). The deepening of chlorophyll-a from 15 to 17 h corresponded with the elevated turbulent dissipation rates mid-water column (10 to 35 m depth). There were also variations of over an order of magnitude in Pseudo-nitzschia spp. counts over short timescales (<1 h; Fig. 4b(1)) that did not correspond with the phase of the tide (Fig. 4a(1)). For example, the total number of cells observed at Station 2 at ~13 h decreased by approximately one order of magnitude before 14 h, and increased again by a factor >25 in the next sample collected at ~14.5 h. Pseudo-nitzschia spp. abundance and dissipation rates at Station 2 were found to increase and decrease in tandem, suggesting that Pseudo-nitzschia spp. was brought to the surface when dissipation increased. To determine if this trend was statistically significant, we calculated the Pearson correlation coefficient. The correlation between the Pseudo-nitzschia spp. data and the  $\log_{10}(\varepsilon)$  was statistically significant (p < 0.05; ~0.58).

At Station 3 Pseudo-nitzschia spp. abundance was relatively constant

and elevated (>10<sup>4</sup> cells/L) throughout the tidal cycle, varying by less than one order of magnitude (Fig. 4b(2)). The chlorophyll-a measurements at Station 3 indicated that the phytoplankton biomass was detected down to depths of 25 m from the surface throughout most of the tidal cycle, with most pronounced abundance toward the end of ebb tide (Fig. 4c(2)). Over the tidal cycle  $\varepsilon$  was consistently greater at Station 3  $(>10^{-7.5} \text{ W/kg from the surface to 20 m depth, Fig. 4c(2))}$  than at Station 2 (dipping below  $10^{-8}$  W/kg, Fig. 4c(1)). The elevated  $\varepsilon$  at Station 3 likely caused Pseudo-nitzschia spp. cell abundance to remain homogenized throughout the tidal cycle and therefore consistently high (>10<sup>4</sup> cells/L) at the surface compared to Station 2 ( $<10^4$  cells/L at  $\sim$ 13 h and  $\sim$ 16 h) (Fig. 4b(1-2)). This is supported by the deeper presence of chlorophyll-a in the water column throughout the tidal cycle at Station 3compared to Station 2. The relation between  $\log_{10}(\varepsilon)$  and Pseudo-nitz*schia* spp. abundance was not statistically significant (p > 0.05;  $\sim -0.68$ ) at Station 3, but this is likely due to  $\varepsilon$  remaining high and inhibiting Pseudo-nitzschia spp. to settle in sub-surface layers as was shown to happen at Station 2 when  $\varepsilon$  was weak. This implies that  $\varepsilon$  and *Pseudo*nitzschia spp. abundance are closely intertwined when turbulence values reach a critical threshold capable of homogenizing the upper water column. Concrete identification of this threshold should be investigated in future studies as it likely varies from system to system depending on stratification conditions and the strength of tidal forcing.

Conceptually, the hydrodynamic observations link to a greater abundance of surface *Pseudo-nitzschia* spp. cells at Station 3 compared to Station 2 in two ways. Station 3 may have greater concentrations of

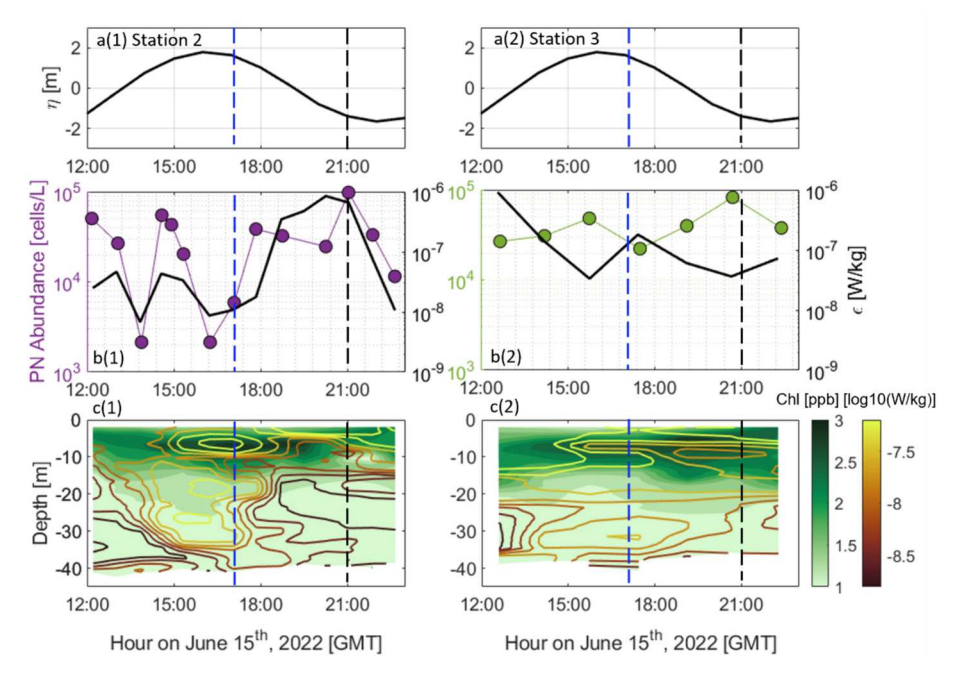


Fig. 4. a (1–2) Variation in the water level observed at NOAA Bar Harbor station (see Fig. 1b), shown twice for reference to subplots b-c. b) On the left axis: abundance of *Pseudo-nitzschia* spp. (PN) measured throughout the tidal cycle at Station 2 (b(1)) and Station 3 (b(2)). On the right axis: turbulent kinetic energy dissipation from the top-most data bin (nearest the surface) at Station 2 (b(1)) and Station 3 (b(2)). c) Chlorophyll-a and turbulence dissipation in the water column throughout the tidal cycle at Station 2 (c(1)) and Station 3 (c(2)). The blue and black dashed lines indicate times 17 h and 21 h respectively as reference for times when dissipation was elevated mid water column (17 h) and restricted to the surface (21 h) at Station 2 and how that compares to values at Station 3.

essential nutrients near-surface, due to consistently higher  $\varepsilon$  which might facilitate transport of nutrients from below the pycnocline to the surface. A second possibility is that the hydrodynamic conditions coincident with Station 3 have the capacity to accumulate or "trap" Pseudonitzschia spp. in a localized area. Entrainment of Pseudo-nitzschia spp. by eddy circulation was a potential mechanism that exacerbated a toxic bloom of P. australis in the Santa Barbara Channel in California (Anderson et al., 2006). P. australis is also the species implicated in the toxic 2016 bloom in the Gulf of Maine (Clark et al., 2019). Overall, these results indicate that surface Pseudo-nitzschia spp. cell abundance is linked to near-surface turbulent dissipation variability throughout the tidal cycle. During the tidal cycle, high  $\varepsilon$  deeper in the water column (>5–10 m; Fig. 2f(2)) was uncoupled with surface turbulence, implying that phytoplankton abundance concentrated below the surface was not yet mixed upwards. Elevated near-surface turbulent dissipation that is uncoupled from bottom-generated dissipation and is not caused by an external source, such as wind, has been shown to occur due to the presence of sub-mesoscale eddies (Spicer and Huguenard, 2020). Surface measurements alone may thereby not provide a complete picture of cell abundance in the water column.

The results from the tidal cycle observations show rotation in the current structure and spatial variability of the turbulent dissipation that suggests the presence of eddies. However, it is impossible to fully resolve the horizontal flow structure with the limited spatial resolution of the tidal velocity measurements. Therefore, we turned to a numerical model of the region to expand the capacity for detection of the flow structure and its changes over time.

#### 4.1.4. Numerical observations on June 15th

The numerically simulated currents and vertical vorticity in Frenchman Bay indicate that horizontal eddies are indeed present in the flow during certain tidal phases on June 15th, 2022 (Fig. 5). Tidal flow enters the bay on flood tide (13 h; Fig. 5a) through two deep channels between islands. One channel is located between Long Porcupine and Bar Island (hereon referred to as the "center channel"; Fig. 5d) and the other between Long Porcupine Island and Stave Island (hereon referred

to as the "right channel"). The friction induced by the islands during flood tide currents results in vorticity consistent with flow separation (Signell and Geyer, 1991; Fig. 5a), a commonly observed flow pattern in the presence of islands and headlands (Wolanski et al., 1984; Geyer and Signell, 1990; Signell and Geyer, 1991). Two counter-rotating flow regions are induced by the islands: one with negative (clockwise) vorticity to the east, and one with positive (counterclockwise) vorticity to the west. An eddy with positive vorticity overlapping with the right channel is formed on the leeward side of Long Island (Fig. 5a). The regions of high vorticity generated in the center channel expand and propagate into the bay by slack tide after flood (16.5 h) and manifest as two counter-rotating eddies just south of the location of the transect (Fig. 5b). During ebb tide and slack after ebb the current velocity vectors are primarily directed out of the bay, but funneling of the tidal flow by bathymetry allows for vorticity to be maintained and surprisingly not reversed with the change of current direction (Fig. 5c-d).

Vorticity in the basin-scale circulation can be transferred to the mean flow (Zimmerman, 1981; Robinson, 1981) a phenomenon known to induce eddies in the residual flow structure, i.e. tidal residual eddies (Pingree, 1978; Zimmerman, 1978, 1981; Robinson, 1981). Therefore, we calculated the depth-averaged residual flow in Frenchman Bay using a least-squares fit of  $\sim$ 7 d surrounding June 15th to the semi-diurnal (12 h), diurnal (24 h) and quarter-diurnal (6 h) tidal harmonics (Fig. 6a). The semi-diurnal harmonic is the dominant tidal harmonic in the region (Alahmed et al., 2022). The quarter-diurnal harmonic was also included in consideration of the highly varied morphometric conditions in the study area that can produce nonlinear interactions of the tidal wave with bathymetry (Parker, 1991). The simulated structure of the residual flows on the northern side of the Porcupine Islands (Fig. 6a) resembles the pattern observed during the slack after flood tide (Fig. 5b). Confirmation of the large eddy on the eastern side of the bay in the residual flow structure supports the hypothesis that the intratidal variability in  $\varepsilon$  at Station 2 (Fig. 2f(2)) is caused by lateral shear induced by tidal flow interactions with bay morphology. Flows are directed through the deep center channel of the bay near Station 2 (see Fig. 1b) and are tidally driven during tidal phases when currents are strong (Fig. 5a and c). The

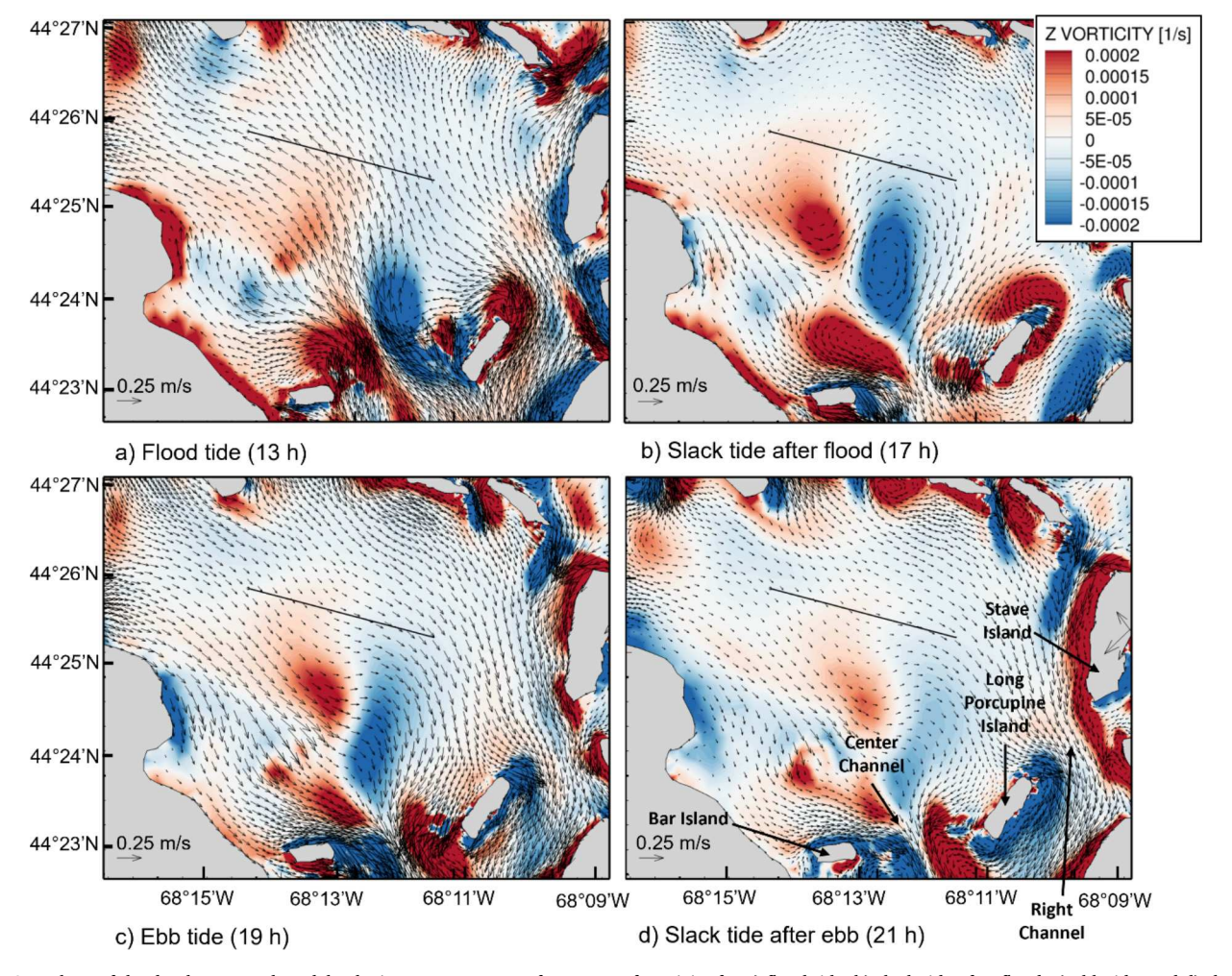


Fig. 5. Snapshots of the depth-averaged model velocity vectors on top of contours of vorticity for a) flood tide, b) slack tide after flood, c) ebb tide, and d) slack tide after ebb. A scale factor of 2000 grid units/magnitude was used for the velocity vectors, and uniform vector spacing was used for visualization purposes. The black line in the bay indicates the location of the transect during the June 15th survey.

residual circulation dominates, and eddies become pronounced when currents weaken on slack tide after flood (Fig. 5b), inducing lateral shear that elevates  $\varepsilon$ . At Station 3 tidal flows are weaker and the eddy circulation in the residual flow is more prominent (Fig. 5a-d) consistently inducing lateral shear that elevates  $\varepsilon$  throughout the tidal cycle (Fig. 2f (3)).

Tidal residual eddies are known to develop because of nonlinear interactions of the tidal flow with coastal geometry including islands (Pingree and Maddock, 1980; Wolanski et al., 1984), headlands (Geyer and Signell, 1990; Signell and Geyer, 1991; Zimmerman, 1981), and bathymetric features (Zimmerman, 1978; Li, 2006; Poul et al., 2016). Poul et al. (2016) schematized the structure of these eddies as a function of bathymetric hills and valleys (their Fig. 2) and demonstrated this structure with numerical simulations (their Fig. 5). The structure of the residual flow observed in Frenchman Bay has remarkable similarity to their illustration of the eddy field induced by bathymetric features (Fig. 6a). Obstruction of the flow by a ledge upstream of the center channel (~44°24'N, -68°14'W), with minimum depths <5 m, not only limits the length scale of the eddy at the eastern end of Bar Island, but also induces a counterclockwise eddy on the leeward side of the hill. The bathymetric slope at the edges of the deep channel and remnants of the glacial lake in the middle of the bay also induce frictional effects on the flow which act to enhance rotation (Robinson, 1981). In summary, the eddies just inside the mouth of the bay are generated by flow constrictions and frictional effects on the tidal flow induced by the islands. However, they are likely maintained, and steered, by the complex

bathymetry, which controls the length scales and spatial positions of the eddies.

The implications of residual flow structures like the observed eddies on material transport depends on how their length scales compare to the oscillatory tidal flow. The circulation patterns can influence the transport of water-borne materials at timescales longer than the tidal cycle if the length scale of a residual eddy exceeds the tidal excursion length,  $L_{tr}$ (Zimmerman, 1979; Robinson, 1981; Alahmed et al., 2022). The tidal excursion length can be quantified as  $L_{tx} = \frac{UT}{\pi}$ , where T and U are the tidal period and tidal current amplitude of the dominant tidal harmonic, respectively (Parsa and Shahidi, 2010). The magnitude of the tidal velocity amplitude of the semi-diurnal harmonic was averaged over the middle of the bay to estimate *U*. For the spring tide period over which the residual flow is shown (Fig. 6a),  $\it U$  is approximately 0.11 m/s. Under these conditions, the major axis of the eddy that appears on the eastern side of the bay in the residual flow (Fig. 6a) has a dimension of approximately  $\sim 3.7$  km, over double  $L_{tx}$  ( $\sim 1.6$  km). This outcome indicates that the eddy will inhibit the flushing of material out of the bay with the tides.

Our findings suggest that the large eddies identified in the depth-averaged residual flow in the bay can accumulate suspended material in the water column, including *Pseudo-nitzschia* spp. Other studies have presented similar findings when investigating eddies at larger scales (Anderson et al., 2006; MacFadyen et al., 2008), like those associated with the Juan de Fuca Eddy (~30–60 km) for example (MacFadyen et al., 2008), or with the transport of oil in the Eastern Mediterranean

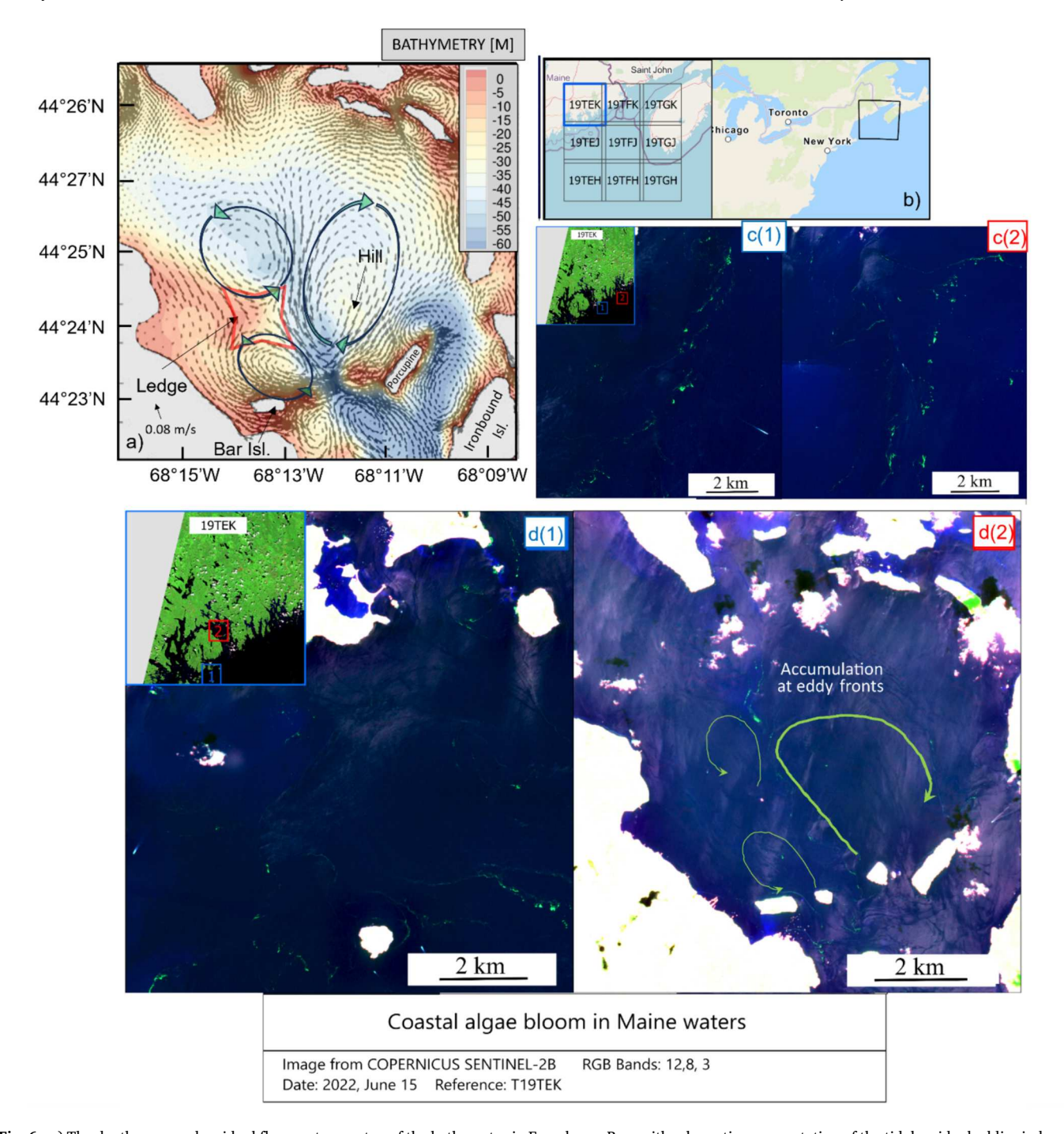


Fig. 6. a) The depth-averaged residual flow vectors on top of the bathymetry in Frenchman Bay, with schematic representation of the tidal residual eddies induced by a ledge at approximately ( $\sim$ 44° 24′N, -68°14′W) and the deep center channel. b) Sentinel-2B Multi-spectral RGB image (bands 12,8,3) examined on June 15th, 2022, in the coast of Maine. c(1) Coastal Maine off of Schoodic Point, c(2) Coastal Maine off of Narraguagus Bay, d(1) Coastal Maine off of Mount Desert Island, and d(2) Frenchman Bay. The green arrows in d(2) were added for emphasis.

Sea (García-Sánchez et al., 2022). The latter study, based on methodology presented in Ramos et al. (2018), found that hyperbolic trajectories, manifesting as counter-circulating eddies coined Lagrangian Coherent Structures (LCS), can accumulate material if the flow field is stable (converging) or disperse material if it is unstable (diverging). The convergence of material in these structures was validated using remote sensing techniques. Utilizing remote sensing methodology, we show Sentinel-2B Multi-spectral RGB images captured in the study region on the date of the tidal survey (June 15th, 2022; Fig. 6b-d). Although it is uncertain whether the phytoplankton identified at the surface were *Pseudo-nitzschia* spp., there is sufficient evidence of filaments and

patches indicating material accumulation offshore (Fig. 6c) and in Frenchman Bay (Fig. 6d). In particular, the convergence of material in the bay loosely depicts the residual eddy structure (Fig. 6a) and follows a similar pattern to the LCS identified in Ramos et al. (2018), further indicating that the convergence zones of the counter-rotating eddies are accumulating material. Counter-rotating eddies at larger scales (>10 km diameter) have been found to locally accumulate phytoplankton in other regions like the southern Gulf of California (Durán-Campos et al., 2019). The present study shows that this phenomenon can also occur at smaller scales (<10 km) in semi-enclosed regions where eddies form due to complex geomorphology. To determine if the accumulation of

phytoplankton by the eddies is relevant at timescales longer than the tide, we consider the weekly sampled *Pseudo-nitzschia* spp. data. We will also discuss the results of the weekly sampled nutrient data, because the availability of specific nutrients can also impact the ability of these diatom species to flourish locally.

#### 4.2. Weekly sampling

#### 4.2.1. Pseudo-nitzschia spp. and nutrients

Pseudo-nitzschia spp. data were collected in July–October of 2021 and 2022 at the 'bay stations' (Stations 2 and 3) located at the center of the bay, and at the 'nearshore stations' (Stave, Sullivan, Jordan, MDIBL and Bar Harbor), which are located closer to the coast (see Fig. 1b). Nutrient data were collected simultaneously at all stations, except for Bar Harbor and MDIBL, and were additionally collected at the three 'stream stations' (Union, Kilkenny, and Egypt). Our reporting focuses on the nutrient concentrations measured in 2022, which included dissolved inorganic nitrogen (DIN:  $\rm NH_3 + NO_x)$  and Si, in addition to TN and TP. The weekly sampled observations allow us to gain insight into the temporal and spatial variability of Pseudo-nitzschia spp. and nutrients in the region.

The concentrations of all measured nutrients (NH<sub>3</sub>, SiO<sub>2</sub>, NO<sub>x</sub>, TN and TP) were first compared qualitatively to the *Pseudo-nitzschia* spp. abundance for the entire sampling period (see Fig. A1 in the Appendix). Largely nutrient concentration values were greater at the 'stream stations' except for NH<sub>3</sub> in Jordan in late August to early September and NO<sub>x</sub> from early September to early October. This spatial trend suggests that freshwater flows are a source of nutrient input to Frenchman Bay. It has been shown that freshwater inflow can be a catalyst for *Pseudo-nitzschia* spp. blooms (Trainer et al., 2012), which could be due to the nutrient loading from the freshwater into coastal waters.

Like all diatoms, Pseudo-nitzschia spp. require silicon to maintain their silicified cell walls and nitrogen for metabolic processes. Studies have focused on understanding the optimal ratio of these nutrients for diatom growth in the marine environment (Gilpin et al., 2004; Egge and Aksnes, 1992). To gain insight to the impact of Si, DIN, and Si:DIN on Pseudo-nitzschia spp. local to Frenchman Bay, we focus specifically on the temporal variability of these constituents at the 'bay station' sampling locations (Stations 2 and 3; Fig. 7). The Si concentrations followed a trend that resembles that of the cell abundance with a lag of approximately 12-14 days between peaks of high Si ( $\sim$ 6-8  $\mu$ mol/L) and maximum cell counts ( $\sim 10^4$ – $10^5$  cells/L; Fig. 7a). The *Pseudo-nitzschia* spp. abundance increased gradually throughout July, over which time Si was depleted (reduced below the detection limit of  $\sim 0.2 \mu mol/L$ ). In only about one week, cell levels decreased by roughly three orders of magnitude ( $\sim 10^5$  to  $\sim 10^2$  cells/L), which could be due to the depletion of Si in the area. DIN concentrations at both Station 2 and 3 were relatively constant ( $\sim$ 2 µmol/L) compared to Si in the early months (July to September), but similarly peaked at the end of September (~7.1 μmol/L at Station 2 and  $\sim$ 5.1  $\mu$ mol/L at Station 3). The Si:DIN appears to trend like Si in the early months (Fig. 7c), but peaks earlier in September at both stations, reaching a maximum (~2.2) in early September at Station 2 and a maximum ( $\sim$ 3.4) in mid-September at Station 3. For the majority of the sampling season, Si:DIN was >1, indicating that nitrogen was potentially limiting diatom growth (Levasseur and Therriault, 1987; Dortch and Whitledge, 1992). However, when Pseudo-nitzschia spp. abundance was greatest in late July and early October, Si was depleted indicating Si limitation, which led to a decline in Pseudo-nitzschia spp. abundance.

To determine if the *Pseudo-nitzschia* spp. statistically correlate with nutrients at the lag periods suggested qualitatively by the observations (Fig. 7), we calculated the sample cross-correlation function for *Pseudo-nitzschia* spp. versus Si, DIN, and Si:DIN, as well as TN and TP for the weekly sampled data at the 'bay stations' (see Fig. A2 in the Appendix). The correlations between *Pseudo-nitzschia* spp. and Si at Station 2 ( $\sim$ 0.39) and Station 3 ( $\sim$ 0.36) fall just below the 85 % confidence

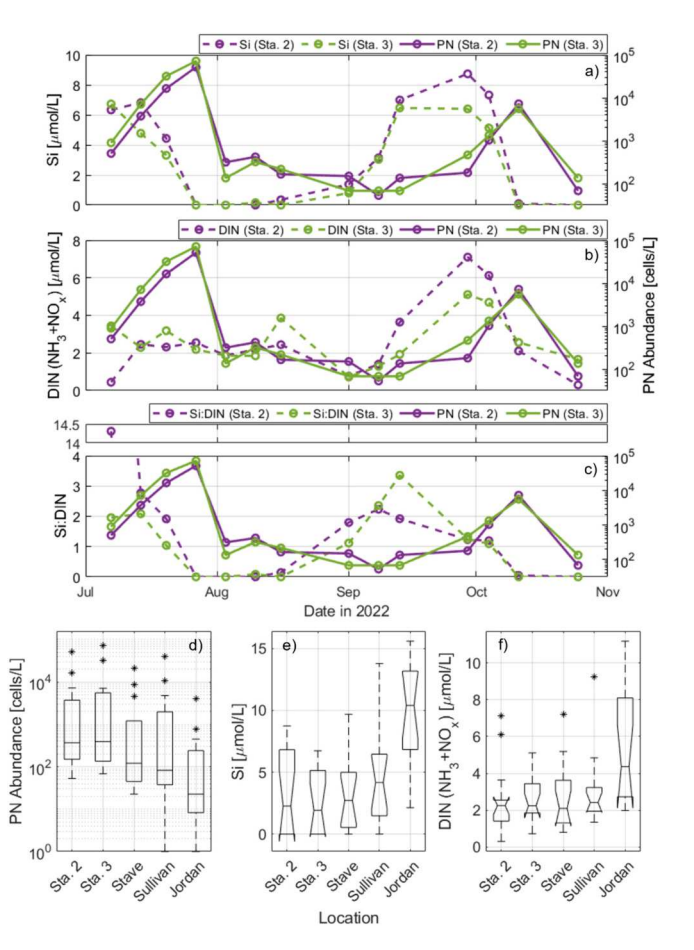


Fig. 7. On the left-axis (dashed lines) of a): silicon concentrations present as dissolved silica, b): dissolved inorganic nitrogen (DIN; as NH<sub>3</sub> + NO<sub>x</sub>) concentrations, and c): ratio of Si to DIN at Station 2 (purple) and Station 3 (green) measured throughout the 2022 sampling season. Note that the y-axis of c) is split between 4 and 14  $\mu$ mol/L for better visualization of the trend. On the right-axis (solid lines) of a-c): Pseudo-nitzschia spp. (PN) abundance at Station 2 (purple) and Station 3 (green) over the same time. d) Box plot of all Pseudonitzschia spp. data measured during the 2022 sampling season at the five stations in the bay. For visualization on a log scale, measurements of 0 cells/L were set to 1 cells/L. e-f) same as d) but for Si concentrations and DIN respectively. The center horizontal line in the box plots is the median, while asterisks denote outliers. Panels e) and f) depict median notches which demonstrate significant differences between station medians at the 95 % confidence level when notches do not overlap. Notches that extend past the interquartile range depicted by the edges of the boxes are due to a small sample size (number of weekly samples) and indicate low confidence (McGill et al., 1978).

interval ( $\sim$ 0.42) at a lag of 13 d, the lag period which was qualitatively estimated from Fig. 7. There is no statistically significant correlation at or above the 85 % CI between *Pseudo-nitzschia* spp. and DIN or Si:DIN for any lag period considered, except for Si:DIN at Station 2 at a lag of 20 d. However, it should be noted that if the first sample date is not considered because the Si:DIN for this sample is an outlier, this relationship is not statistically significant at a lag of 20 d, but is significant within the 85 % CI at a lag of 13 d (not shown).

The low correlations between the *Pseudo-nitzschia* spp. and the measured nutrients could be a result of limitations of our dataset. Because only *Pseudo-nitzschia* spp. were enumerated, it is possible that the variations in the nutrient concentrations were a result of competition by other phytoplankton species. An Si concentration of 2 µmol/L has been proposed as a threshold at which diatoms will dominate (Egge and Aksnes, 1992), and our concentrations were often below this value, indicating that a different type of phytoplankton, like dinoflagellates, might have been present and dominant. Further, because silicate and

nitrate depletion can occur on the order of days (Gilpin et al., 2004), the sampling resolution of our weekly sampled data might be too coarse to result in high correlations, even if such correlations existed.

The spatial variability of Pseudo-nitzschia spp., Si, and DIN in the study area (Fig. 7d-f) suggests that Pseudo-nitzschia spp. has greatest abundance in the middle of the bay at the 'bay stations' (Stations 2 and 3; Fig. 7d), though the medians at these stations were not significantly different from the other stations. Median notches computed using MathWorks' MATLAB software, based on the method of McGill et al. (1978), were used to assess significant differences between station medians at the 95 % confidence interval for Pseudo-nitzschia spp., Si, and DIN, however these notches are not shown for Pseudo-nitzschia spp. because the data are best visualized on a log-scale due to outliers >10<sup>4</sup> cells/L. At the 'bay stations', the Si concentrations are also lowest (Fig. 7e), but only the Jordan station is significantly different from the other stations, with the highest concentrations of Si. The DIN at the 'bay stations' compares to the 'nearshore stations', except for the Jordan station, which is furthest from the open ocean (Fig. 1b) and has higher levels of DIN, although this difference is not statistically significant based on the median (Fig. 7f). The lower concentrations of Si at Station 2 and Station 3 are speculated to be a result of depletion by the higher abundance of Pseudo-nitzschia spp., due to accumulation of Pseudonitzschia spp. at the 'bay stations', as observed during the tidal cycle survey on June 15th, 2022. The correlation between Pseudo-nitzschia spp. and Si over the weekly sampling period falling just short of the 85 % CI is possibly a result of the limitations discussed earlier, therefore we

cannot confirm that *Pseudo-nitzschia* spp. are the main factor influencing Si depletion. However, to confirm that *Pseudo-nitzschia* spp. accumulate at the 'bay stations' over timescales longer than one tidal cycle due to the residual eddies, we considered the weekly sampled *Pseudo-nitzschia* spp. abundance data from both 2021 and 2022.

In 2021, the median Pseudo-nitzschia spp. abundance at Station 2, Station 3, and the Sullivan station were significantly greater than the medians at the Jordan and MDIBL stations (not shown), which are located near the coast, furthest from the outer ocean (Fig. 1b). There were no significant differences between station medians in 2022, however weekly average cell counts over the sampling season at each station indeed document the highest abundance of Pseudo-nitzschia spp. occurring at Stations 2 and 3, in the middle of the bay in both 2021 (Fig. 8a) and 2022 (Fig. 8b). Conclusions from Clark et al. (2019) lead to an assumption that Pseudo-nitzschia spp. enter the bay from the outer Gulf of Maine. Following that assumption, higher cell concentrations in the center of the bay compared to the Bar Harbor station located on the ocean side of the Porcupine Islands (Fig. 1b) support a conclusion that the observed eddies have capacity to drive localized accumulation of Pseudo-nitzschia spp. cells, causing higher concentrations in the bay center despite greater distance from the Gulf when compared to Bar Harbor. Although the results of the tidal cycle survey indicate that surface measured Pseudo-nitzschia spp. concentrations are strongly linked to near-surface turbulence, higher levels of cell abundance at Stations 2 and 3 compared to nearshore at these longer timescales indicates that residual flows also play a role in the spatial distribution of

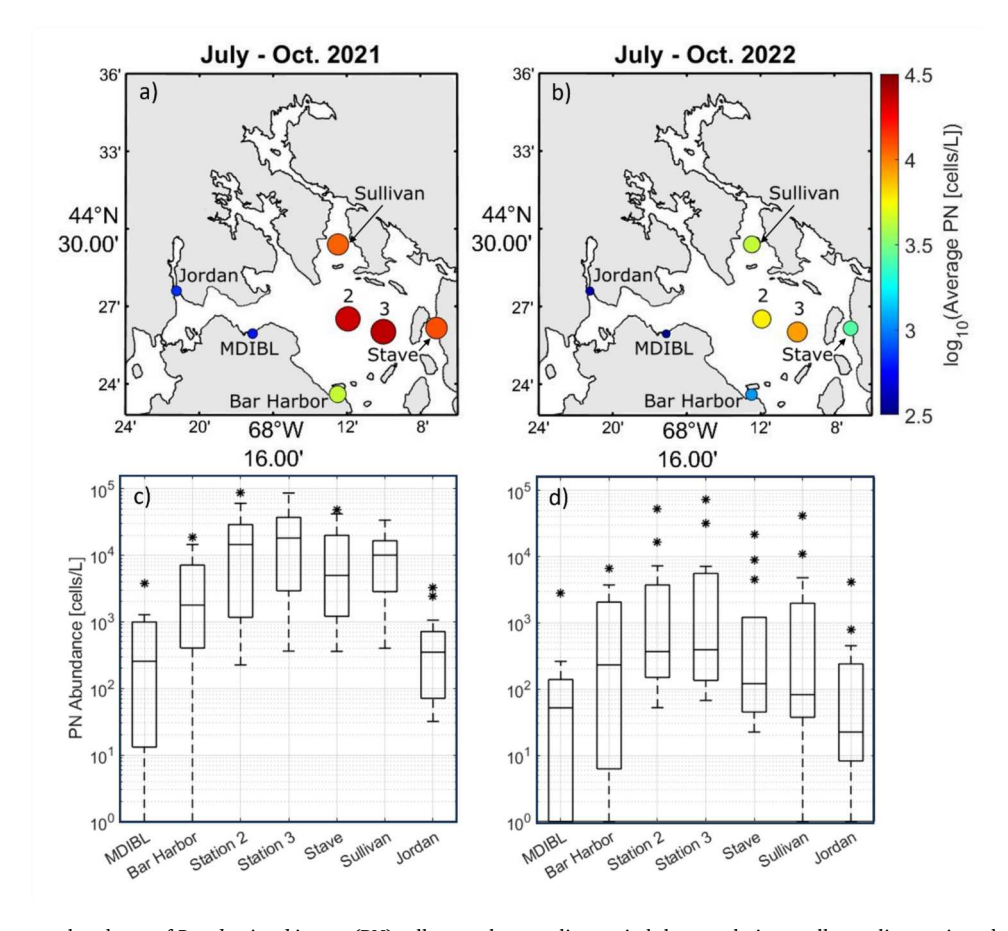


Fig. 8. Top panels: Average abundance of *Pseudo-nitzschia* spp. (PN) cells over the sampling period shown relative to all sampling stations during July–October in a) 2021 and b) 2022. MEDMR's sampling data collected in the sampling window at their Bar Harbor and MDIBL stations were also included. The color and size of the circles represent the average *Pseudo-nitzschia* spp. cell concentrations in cells/L (size of circles was based on log<sub>10</sub>(cells/L) scaled by a power of 4.2 to visualize differences in abundance). Bottom panels: Box plots of the data collected during the sampling period at the seven stations shown in a) and b) for c) 2021 and d) 2022 respectively. The center horizontal line in the box plots is the median, while asterisks denote outliers. For visualization on a log scale, measurements of 0 cells/L were set to 1 cells/L.

the cell abundance.

#### 4.3. Implications for monitoring & management

This study demonstrates the formation of residual eddies due to tidal flow interactions with legacy geomorphic attributes related to a postglacial lake formed during the retreat of the Laurentide ice sheet from Maine's modern coastal area (Borns, 1973 and references therein; Borns et al., 2004; Braun and Braun, 2016). The mechanism responsible for eddy formation is lateral shear of the tidal currents caused by flow interactions with islands at the mouth of the bay and bathymetric gradients within the bay that steer tidal flows. These eddies were found to be relevant for the horizontal distribution of algae, leading to the accumulation of algal cells at the periphery of the eddies, a phenomenon observed in other regions of the world, but at larger scales (Coria-Monter et al., 2014). The accumulation of phytoplankton by the eddies was also shown to be relevant at timescales longer than the tide. These findings are important because they both inform the spatial scales over which local HAB monitoring should take place and indicate the potential for algal "hot spots" to form in other similarly complex coastal estuaries where transient eddies could form around islands, underwater hills, and headlands. However, an important outcome from the weekly nutrient sampling was the observed depletion of Si by Pseudo-nitzschia spp., followed by a rapid decline in the *Pseudo-nitzschia* spp. population within one to two weeks at the 'bay stations', where the residual eddies were observed. It is possible that with greater sampling frequency, we would have detected even greater peaks in Pseudo-nitzschia spp. abundance, as growth rates are on the order of days (Morse et al., 2014). Indeed, similar patterns between diatom species and Si have been observed in other studies, with Si depletion occurring over timescales on the order of days (Gilpin et al., 2004). These timescales might be of particular concern in regions where local circulation patterns aid the accumulation of algal cells because accumulation might continue for some time (days) in nutrient depleted zones, leading to stress on the diatoms. This is especially important in the context of Pseudo-nitzschia spp. and Si, as insufficient Si availability is thought to be a trigger for toxin production in these diatoms (Bates et al., 1998). Yet, it is well recognized that the relation between cell abundance and toxin production is not straightforward (Anderson et al., 2006; Trainer et al., 2012), and despite the observed increases in Pseudo-nitzschia spp. in conjunction with Si, insufficient levels of domoic acid, the toxin produced by the species, were detected in regular monitoring to indicate the presence of a HAB (personal communication with MEDMR, December 4, 2023). However, these results do provide some support for nutrient monitoring in addition to diatom monitoring, and for possibly increasing monitoring frequency in localized 'hot spot' areas known for material accumulation.

Further, the comparison of turbulent dissipation rates and *Pseudonitzschia* spp. measurements collected during the June 15th tidal cycle survey suggests that near-surface mixing can influence the depth of algal cells. Elevated near-surface  $\varepsilon$  generated by eddies or other processes such as wind shear can disperse algal cells into a monitoring zone. Conversely, low  $\varepsilon$  might reduce the near-surface concentration despite potentially large cell density below the monitoring zone. This finding implies that surface monitoring alone might not provide a complete picture of *Pseudo-nitzschia* spp. abundance in a local area. Overall, the findings detailed in this study provide incentive to examine current practices of HAB monitoring and management, especially to consider the linkages between coastal geomorphology and hydraulic conditions influencing HAB sampling outcomes, and the influence of millennial time scales on modern hydraulic conditions.

# 4.4. Study limitations

In this study, two-dimensional (depth-averaged) numerical simulations were used to focus on large-scale circulation features like the eddies in the center of the bay. We have confidence that the two-

dimensional model output was appropriate because the depthaveraged results match the observations well and because Frenchman Bay is primarily barotropically (tidally) driven with small freshwater inputs and large tidal ranges. However, some vertical variation in the density and current structure was observed in the tidal cycle measurements when the eddies formed (Figs. 2 and 3), indicating that further insight could be gained from three-dimensional investigations. An understanding of the strength of the eddy circulation with depth could also help to refine the range of depths at which algal cell accumulation occurs and therefore monitoring should take place. Greater spatial resolution in the observations could provide more insight into the spatial structure of the local circulation features, although such resolution is difficult to obtain in the field. It should also be noted that there are two small islands between Bar Island and Long Porcupine Island (Fig. 1b) that are incorporated into the model bathymetry data, and are therefore included as topographic features, but are not included as closed boundaries in the model domain. These features could result in the enhancement of the modeled velocity over those regions (Fig. 5a). However, these local phenomena are not believed to impact our overall findings because our investigation of the vorticity and residual flow is primarily focused on the center of the bay.

#### 5. Conclusions

There are two main findings of this study. The first is that surface Pseudo-nitzschia spp. abundance is linked to elevated near-surface turbulent dissipation, indicating that surface monitoring alone may not be sufficient to understand the temporal and spatial scales of some harmful algal bloom species. The second is that tidal flow interactions with islands and sharp bathymetric gradients in Frenchman Bay produced both transient and residual eddies that elevated near-surface turbulent dissipation and accumulated Pseudo-nitzschia spp. cells. These vortical structures were produced by tidal hydraulics interacting with coastal geomorphology, and were advected into the middle of the bay during flood tide. There, the eddies enhanced turbulent dissipation at some locations, leading to increased Pseudo-nitzschia spp. cell counts, measured at the water surface. The vorticity that presents as counterrotating submesoscale eddies in the center of the bay persists in the residual flow structure. These residual eddies accumulate material such as Pseudo-nitzschia spp. since the eddy length scale is greater than the tidal excursion length. The accumulation of material was reinforced by satellite images showing dense zones of phytoplankton on the eddy periphery, or 'convergence zones,' on the day of the tidal cycle survey. Annual Pseudo-nitzschia spp. sampling also supports accumulation of algae over longer timescales in the middle of the bay compared to the surrounding estuaries and locations closer to the ocean boundary.

Our results suggest that silica concentrations might be an important factor controlling the temporal variability in *Pseudo-nitzschia* spp. abundance in Frenchman Bay, however more frequent sampling in future investigations is necessary to confirm this. The results of this study in general provide motivation to revisit current monitoring and management strategies for HABs. Revised strategies responding to these observations would consider associations between coastal geomorphology and tidal hydraulic conditions, and how these linkages can influence material accumulation patterns in estuaries in deglaciated coastal settings.

# Funding

This material is based upon work supported by the U.S. Geological Survey under Grant/Cooperative Agreement No. G21AP10179-00, Maine Outdoor Heritage Fund Contract No. CT09A20220531\*3098, National Science Foundation (NSF) Grant Number 2045866, administrative assistance from the Maine Water Resources Research Institute in the Sen. George J. Mitchell Center, and student support from the Maine Agricultural and Forest Experiment Station. Iván Pérez-Santos was

funded by FONDECYT 1211037, COPAS COASTAL FB210021, and CIEP R20F002. The views and conclusions contained in this document are those of the authors and should not be interpreted as representing the opinions or policies of the U.S. Geological Survey. Mention of trade names or commercial products does not constitute their endorsement by the U.S. Geological Survey. This manuscript is submitted for publication with the understanding that the United States Government is authorized to reproduce and distribute reprints for Governmental purposes.

## CRediT authorship contribution statement

Taylor Bailey: Writing – review & editing, Writing – original draft, Visualization, Validation, Resources, Methodology, Investigation, Formal analysis, Data curation, Conceptualization. Lauren Ross: Writing – review & editing, Writing – original draft, Visualization, Supervision, Resources, Project administration, Methodology, Investigation, Funding acquisition, Formal analysis, Data curation, Conceptualization. Nicholas Tiner: Writing – review & editing, Writing – original draft, Methodology, Investigation, Data curation. Sean M.C. Smith: Writing – review & editing, Resources, Methodology, Funding acquisition, Data curation, Conceptualization. Iván Ernesto Pérez Santos: Writing – review & editing, Investigation. Antonio Ramos: Visualization, Methodology, Data curation, Conceptualization. Alejandro García Mendoza: Visualization, Methodology, Data curation, Conceptualization. David Miller: Writing – review & editing, Methodology.

#### Declaration of competing interest

The authors declare the following financial interests/personal relationships which may be considered as potential competing interests: Co-author David Miller works for the Maine Department of Marine Resources who monitor for harmful algal blooms in Maine. If there are other authors, they declare that they have no known competing financial interests or personal relationships that could have appeared to influence the work reported in this paper.

## Data availability

Data will be made available on request.

## Acknowledgments

We would like to thank Gary Shenk, Charles Culbertson, and Thomas Huntington from the United States Geological Survey for guidance during the design of our overarching HABs research project in the Frenchman Bay area, Rob Wilpan, Chairman of the Town of Sorrento Board of Selectman, for project guidance, feedback, and outreach, Katherine Hubbard and Christina Chadwick at Florida Fish and Wildlife Conservation Commission for their help processing the Pseudo-nitzschia spp. measurements from the June 15th survey, and Neil Fisher, Hayden Libby, and Danielle Martin for their help with the tidal cycle fieldwork. We would also like to thank Acadia Aquafarms and Waukeag Neck Oyster Farm in the Frenchman Bay region for allowing us to use their aquaculture lease sites for data collection. And thanks to Dr. Tom Hope for allowing us to use his mussel platform for data collection. We would like to thank and acknowledge support for this project from the Town of Bar Harbor, Frenchman Bay United, the John C. and Elisabeth B. Cochran Family Fund, and Friends of Frenchman Bay. Thank you to the Maine Department of Marine Resources for their help during the two years of summer sampling, teaching us how to monitor Pseudo-nitzschia spp. and allowing us to use their equipment, and for letting us keep our boat on their property. Thank you as well to Hanna Cronin for processing the 2021 Pseudo-nitzschia spp. samples, and Gilbert and Silvia Lamb for helping facilitate our safe access to Frenchman Bay for field measurements. Thank you to Carol Pollard at VIMS Analytical Services

Center and Scott Lariviere at the UMaine Sawyer Water Research Lab for guidance with the nutrient sampling. Lastly, we thank the three anonymous reviewers whose valuable comments and feedback greatly contributed to the improvement of our manuscript.

#### Appendix A. Supplementary data

Supplementary data to this article can be found online at https://doi.org/10.1016/j.scitotenv.2024.174902.

#### References

- Alahmed, S., Ross, L., Smith, S.M.C., 2022. Coastal hydrodynamics and timescales in meso-macrotidal estuaries in the Gulf of Maine: a model study. Estuar. Coasts 45 (7), 1888–1908. https://doi.org/10.1007/s12237-022-01067-9.
- Anderson, D.M., 2009. Approaches to monitoring, control and management of harmful algal blooms (HABs). Ocean Coast. Manag. 52 (7), 342. https://doi.org/10.1016/j. ocecoaman.2009.04.006.
- Anderson, D.M., Andersen, P., Bricelj, V.M., Cullen, J.J., Rensel, J.E., 2001. Monitoring and management strategies for harmful algal blooms in coastal waters. In: APEC #201-MR-01.1, Asia Pacific Economic Program, Singapore, and Intergovernmental Oceanographic Commission Technical Series No. 59, Paris.
- Anderson, C.R., Brzezinski, M.A., Washburn, L., Kudela, R., 2006. Circulation and environmental conditions during a toxigenic Pseudo-nitzschia australis bloom in the Santa Barbara Channel, California. Mar. Ecol. Prog. Ser. 327, 119–133.
- Bates, S.S., Garrison, D.L., Horner, R.A., 1998. Bloom dynamics and physiology of domoic-acid-producing *Pseudo-nitzschia* species. Nato Asi Ser. G Ecol. Sci. 41, 267–292.
- Bates, S.S., Hubbard, K.A., Lundholm, N., Montresor, M., Leaw, C.P., 2018. Pseudonitzschia, Nitzschia, and domoic acid: new research since 2011. Harmful Algae 79, 3–43. https://doi.org/10.1016/j.hal.2018.06.001.
- Borns Jr., H.W., Doner, L.A., Dorion, C.C., Jacobson Jr., G.L., Kaplan, M.R., Kreutz, K.J., Lowell, T.V., Thompson, W.B., Weddle, T.K., 2004. The deglaciation of Maine, USA. In: Developments in Quaternary Sciences, 2, pp. 89–109. https://doi.org/10.1016/ S1571-0866(04)80190-8.
- Borns Jr., H.W., 1973. Late Wisconsin fluctuations of the Laurentide Ice Sheet in southern and eastern New England. In: Black, R.F., Goldthwait, R., Willman, H.B. (Eds.), The Wisconsinan Stage. Geological Society of America, Memoir, 136, pp. 37–45. https://doi.org/10.1130/MEM136-p37.
- Box, G.E.P., Jenkins, G.M., Reinsel, G.C., 1994. Time Series Analysis: Forecasting and Control, 3rd edition. Prentice Hall, Englewood Cliffs, NJ.
- Braun, D., Braun, D., 2016. Guide to the Geology of Mount Desert Island and Acadia National Park. North Atlantic Books, Berkeley, California, USA, pp. 54–59.
- Brooks, D.A., Baca, M.W., Lo, Y.T., 1999. Tidal circulation and residence time in a macrotidal estuary: Cobscook Bay, Maine. Estuar. Coast. Shelf Sci. 49 (5), 647–665. https://doi.org/10.1006/ecss.1999.0544.
- Clark, S., Hubbard, K.A., Anderson, D.M., McGillicuddy Jr., D.J., Ralston, D.K., Townsend, D.W., 2019. Pseudo-nitzschia bloom dynamics in the Gulf of Maine: 2012–2016. Harmful Algae 88, 101656. https://doi.org/10.1016/j. hal.2019.101656.
- Coria-Monter, E., Monreal-Gómez, M.A., Salas-de-León, D.A., Aldeco-Ramírez, J., Merino-Ibarra, M., 2014. Differential distribution of diatoms and dinoflagellates in a cyclonic eddy confined in the Bay of La Paz, Gulf of California. J. Geophys. Res. Oceans 119 (9), 6258–6268.
- Coria-Monter, E., Monreal-Gómez, M.A., de León, D.A.S., Durán-Campos, E., Merino-Ibarra, M., 2017. Wind driven nutrient and subsurface chlorophyll-a enhancement in the Bay of La Paz, Gulf of California. Estuar. Coast. Shelf Sci. 196, 290–300. https://doi.org/10.1002/2014/C009916.
- Davies, J.L., 1964. A morphogenic approach to world shorelines. Z. Geomorphol. 127–142.
- Dortch, Q., Whitledge, T.E., 1992. Does nitrogen or silicon limit phytoplankton production in the Mississippi River plume and nearby regions? Cont. Shelf Res. 12 (11), 1293–1309.
- Dudley, R.W., 2015. Regression equations for monthly and annual mean and selected percentile streamflows for ungaged rivers in Maine. In: U.S. Geological Survey Scientific Investigations Report 2015–5151, p. 35. https://doi.org/10.3133/ sir20155151.
- Durán-Campos, E., Monreal-Gómez, M.A., de León, D.A.S., Coria-Monter, E., 2019. Impact of a dipole on the phytoplankton community in a semi-enclosed basin of the southern Gulf of California, Mexico. Oceanologia 61 (3), 331–340. https://doi.org/ 10.1016/j.oceano.2019.01.004.
- Egbert, G.D., Erofeeva, S.Y., 2002. Efficient inverse modeling of barotropic ocean tides. J. Atmos. Ocean. Technol. 19 (2), 183–204. https://doi.org/10.1175/1520-0426 (2002)019<0183:EIMOBO>2.0.CO;2.
- Egge, J.K., Aksnes, D.L., 1992. Silicate as a regulating nutrient in phytoplankton competition. Mar. Ecol. Prog. Ser. 83, 281–289.
- FAO, 2022. The State of World Fisheries and Aquaculture 2022. Towards Blue Transformation. FAO, Rome. https://doi.org/10.4060/cc0461en.
- García-Sánchez, G., Mancho, A.M., Ramos, A.G., Coca, J., Wiggins, S., 2022. Structured pathways in the turbulence organizing recent oil spill events in the Eastern Mediterranean. Nature Sci. Rep. https://doi.org/10.1038/s41598-022-07350-w.

- Gentien, P., Donaghay, P., Yamazaki, H., Raine, R., Reguera, B., Osborn, T., 2005. Harmful algal blooms stratified. Oceanography 18 (2).
- Geyer, W.R., Signell, R., 1990. Measurements of tidal flow around a headland with a shipboard acoustic Doppler current profiler. J. Geophys. Res. Oceans 95 (C3), 3189–3197. https://doi.org/10.1029/JC095iC03p03189.
- Gilpin, L.C., Davidson, K., Roberts, E., 2004. The influence of changes in nitrogen: silicon ratios on diatom growth dynamics. J. Sea Res. 51 (1), 21–35. https://doi.org/ 10.1016/j.seares.2003.05.005.
- Glibert, P.M., Anderson, D.M., Gentien, P., Granéli, E., Sellner, K.G., 2005. The Global, Complex Phenomena of Harmful Algal Blooms. https://doi.org/10.5670/ oceanog.2005.49.
- Levasseur, M.E., Therriault, J.C., 1987. Phytoplankton biomass and nutrient dynamics in a tidally induced upwelling: the role of the NO3: SiO4 ratio. Mar. Ecol. Prog. Ser. 39, 87-97.
- Li, C., 2006. Modeling of bathymetry-locked residual eddies in well-mixed tidal channels with arbitrary depth variations. J. Phys. Oceanogr. 36 (10), 1974–1993. https://doi. org/10.1175/JPO2955.1.
- Li, C., Weeks, E., 2009. Measurements of a small scale eddy at a tidal inlet using an unmanned automated boat. J. Mar. Syst. 75 (1–2), 150–162. https://doi.org/ 10.1016/j.jmarsys.2008.08.007.
- MacFadyen, A., Hickey, B.M., Foreman, M.G., 2005. Transport of surface waters from the Juan de Fuca eddy region to the Washington coast. Cont. Shelf Res. 25 (16), 2008–2021. https://doi.org/10.1016/j.csr.2005.07.005.
- MacFadyen, A., Hickey, B.M., Cochlan, W.P., 2008. Influences of the Juan de Fuca Eddy on circulation, nutrients, and phytoplankton production in the northern California current system. J. Geophys. Res. Oceans 113 (C8). https://doi.org/10.1029/ 2007/10.004412
- Maine, 2022a. Aquaculture Map: Department of Marine Resources. Maine.gov. https://www.maine.gov/dmr/aquaculture/maine-aquaculture-leases-and-lpas/aquaculture-web-map.
- Maine, 2022b. Biotoxins in Maine: Department of Marine Resources. Maine.gov. https://www.maine.gov/dmr/fisheries/shellfish/bureau-of-public-health-programs/biotoxins-in-maine.
- McGill, R., Tukey, J.W., Larsen, W.A., 1978. Variations of box plots. Am. Stat. 32 (1), 12–16
- Morse, R.E., Mulholland, M.R., Egerton, T.A., Marshall, H.G., 2014. Phytoplankton and nutrient dynamics in a tidally dominated eutrophic estuary: daily variability and controls on bloom formation. Mar. Ecol. Prog. Ser. 503, 59–74. https://doi.org/ 10.3354/meps10743.
- National Centers for Environmental Information. (n.d.). Local Climatological Data Station Details Bar Harbor Airport, ME US. National Oceanic and Atmospheric Administration. https://www.ncei.noaa.gov/cdo-web/datasets/LCD/stations/WBAN:14616/detail.
- National Oceanic and Atmospheric Administration. (n.d.) Meteorological observations NOAA tides & currents. https://www.tidesandcurrents.noaa.gov/met.html?id = 8413320.
- Parker, B.B. (Ed.), 1991. Tidal Hydrodynamics. John Wiley & Sons.
- Parsa, J., Shahidi, A.E., 2010. Prediction of tidal excursion length in estuaries due to the environmental changes. Int. J. Environ. Sci. Technol. 7 (4), 675–686. https://doi. org/10.1007/BF03326177.
- Pawlovicz, R., 2020. "M\_Map: A mapping package for MATLAB", version 1.4m, [computer software]. available online at. www.eoas.ubc.ca/~rich/map.html.
- Pingree, R.D., 1978. The formation of the shambles and other banks by tidal stirring of the seas. J. Mar. Biol. Assoc. United Kingdom 58 (1), 211–226. https://doi.org/ 10.1017/S0025315400024504
- Pingree, R.D., Maddock, L., 1980. Tidally induced residual flows around an island due to both frictional and rotational effects. Geophys. J. Int. 63 (2), 533–546. https://doi. org/10.1111/j.1365-246X.1980.tb02636.x.
- Pitcher, G.C., Figueiras, F.G., Hickey, B.M., Moita, M.T., 2010. The physical oceanography of upwelling systems and the development of harmful algal blooms. Prog. Oceanogr. 85 (1–2), 5–32. https://doi.org/10.1016/j.pocean.2010.02.002.

- Poul, H.M., Backhaus, J., Dehghani, A., Huebner, U., 2016. Effect of subseabed salt domes on tidal residual currents in the Persian Gulf. J. Geophys. Res. Oceans 121 (5), 3372–3380. https://doi.org/10.1002/2015JC011421.
- Qin, Q., Shen, J., 2019. Physical transport processes affect the origins of harmful algal blooms in estuaries. Harmful Algae 84, 210–221. https://doi.org/10.1016/j. hal.2019.04.002.
- Ramos, A.G., García-Garrido, V.J., Mancho, A.M., Wiggins, S., Coca, J., Glenn, S., Schofield, O., Kohut, J., Aragon, D., Kerfoot, J., Haskins, T., Miles, T., Haldeman, C., Strandskov, N., Allsup, B., Jones, C., Shapiro, J., 2018. Lagrangian coherent structure assisted path planning for transoceanic autonomous underwater vehicle missions. Nature Sci. Rep. https://doi.org/10.1038/s41598-018-23028-8.
- Robinson, I.S., 1981. Tidal vorticity and residual circulation. Deep Sea Res. A. Oceanogr. Res. Papers 28 (3), 195–212. https://doi.org/10.1016/0198-0149(81)90062-5.
- Ross, L., Huguenard, K.D., Sottolichio, A., 2019. Intratidal and fortnightly variability of vertical mixing in a macrotidal estuary: the Gironde. J. Geophys. Res. Oceans 124, 2641–2659. https://doi.org/10.1029/2018JC014456.
- Ross, L., Alahmed, S., Smith, S.M., Roberts, G., 2021. Tidal and subtidal transport in short, tidally-driven estuaries with low rates of freshwater input. Cont. Shelf Res. 224, 104453 https://doi.org/10.1016/j.csr.2021.104453.
- Salas-de-León, D.A., Carbajal, N., Monreal-Gómez, M.A., Gil-Zurita, A., 2011. Vorticity and mixing induced by the barotropic M2 tidal current and zooplankton biomass distribution in the Gulf of California. J. Sea Res. 66 (2), 143–153. https://doi.org/ 10.1016/j.seares.2011.05.011.
- Signell, R.P., Geyer, W.R., 1991. Transient eddy formation around headlands.
- J. Geophys. Res. Oceans 96 (C2), 2561–2575. https://doi.org/10.1029/90JC02029.Spicer, P., Huguenard, K., 2020. Observations of near-surface mixing behind a headland.J. Mar. Sci. Eng. 8 (2), 68. https://doi.org/10.3390/jmse8020068.
- Trainer, V.L., Hickey, B.M., Horner, R.A., 2002. Biological and physical dynamics of domoic acid production off the Washington coast. Limnol. Oceanogr. 47 (5), 1438–1446. https://doi.org/10.4319/lo.2002.47.5.1438.
- Trainer, V.L., Hickey, B.M., Lessard, E.J., Cochlan, W.P., Trick, C.G., Wells, M.L., MacFadyen, A., Moore, S.K., 2009. Variability of Pseudo-nitzschia and domoic acid in the Juan de Fuca eddy region and its adjacent shelves. Limnol. Oceanogr. 54 (1), 289–308. https://doi.org/10.4319/lo.2009.54.1.0289.
- Trainer, V.L., Bates, S.S., Lundholm, N., Thessen, A.E., Cochlan, W.P., Adams, N.G., Trick, C.G., 2012. Pseudo-nitzschia physiological ecology, phylogeny, toxicity, monitoring and impacts on ecosystem health. Harmful Algae 14, 271–300. https://doi.org/10.1016/j.hal.2011.10.025.
- Trinast, E.M., 1975. Tidal currents and Acartia distribution in Newport Bay, California. Estuar. Coast. Mar. Sci. 3 (2), 165–176. https://doi.org/10.1016/0302-3524(75)
- U.S. Geological Survey, 2019. The StreamStats Program. USGS. https://streamstats.usgs.
- Willmott, C.J., 1981. On the validation of models. Phys. Geogr. 2 (2), 184–194. https://doi.org/10.1080/02723646.1981.10642213.
- Wolanski, E., Imberger, J., Heron, M.L., 1984. Island wakes in shallow coastal waters. J. Geophys. Res. Oceans 89 (C6), 10553–10569. https://doi.org/10.1029/ JC089iC06p10553.
- Yang, Z., Wang, T., 2013. Tidal residual eddies and their effect on water exchange in Puget Sound. Ocean Dyn. 63, 995–1009. https://doi.org/10.1007/s10236-013-0635-7
- Zimmerman, J.T.F., 1978. Topographic generation of residual circulation by oscillatory (tidal) currents. Geophys. Astrophys. Fluid Dyn. 11 (1), 35–47. https://doi.org/ 10.1080/03091927808242650.
- Zimmerman, J.T.F., 1979. On the Euler-Lagrange transformation and the Stokes' drift in the presence of oscillatory and residual currents. Deep Sea Res. Part A. Oceanogr. Res. Pap. 26 (5), 505–520. https://doi.org/10.1016/0198-0149(79)90093-1.
- Zimmerman, J.T.F., 1981. Dynamics, diffusion and geomorphological significance of tidal residual eddies. Nature 290 (5807), 549–555. https://doi.org/10.1038/ 290549a0.